



Royal Netherlands Academy of Arts and Sciences (KNAW) KONINKLIJKE NEDERLANDSE AKADEMIE VAN WETENSCHAPPEN

Inhibition of stress resilience and adult hippocampal neurogenesis by platelet-derived LPA16:0 in anxiety

Larrieu, Thomas; Grieco, Fabio; Carron, Charline; Vilademunt, Marta; Weber, Crystal; Ginggen, Kyllian; Delacrétaz, Aurélie; Gallart-Ayala, Hector; Tsuda, Mumeko C; Cameron, Heather A; Eap, Chin B; Ivanisevic, Julijana; Magistretti, Pierre; Salta, Evgenia; Tosoni, Giorgia; Ayyildiz, Dilara; Telley, Ludovic; Dayer, Alexandre; Pigué, Camille; Toni, Nicolas

published in

Nature Communications
2026

DOI (link to publisher)

[10.1038/s41467-026-69240-3](https://doi.org/10.1038/s41467-026-69240-3)

document version

Publisher's PDF, also known as Version of record

[Link to publication in KNAW Research Portal](#)

citation for published version (APA)

Larrieu, T., Grieco, F., Carron, C., Vilademunt, M., Weber, C., Ginggen, K., Delacrétaz, A., Gallart-Ayala, H., Tsuda, M. C., Cameron, H. A., Eap, C. B., Ivanisevic, J., Magistretti, P., Salta, E., Tosoni, G., Ayyildiz, D., Telley, L., Dayer, A., Pigué, C., & Toni, N. (2026). Inhibition of stress resilience and adult hippocampal neurogenesis by platelet-derived LPA16:0 in anxiety. *Nature Communications*. Advance online publication. <https://doi.org/10.1038/s41467-026-69240-3>

General rights

Copyright and moral rights for the publications made accessible in the public portal are retained by the authors and/or other copyright owners and it is a condition of accessing publications that users recognise and abide by the legal requirements associated with these rights.

- Users may download and print one copy of any publication from the KNAW public portal for the purpose of private study or research.
- You may not further distribute the material or use it for any profit-making activity or commercial gain.
- You may freely distribute the URL identifying the publication in the KNAW public portal.

Take down policy

If you believe that this document breaches copyright please contact us providing details, and we will remove access to the work immediately and investigate your claim.

E-mail address:
pure@knaw.nl

Inhibition of stress resilience and adult hippocampal neurogenesis by platelet-derived LPA16:0 in anxiety

Received: 20 January 2025

Accepted: 27 January 2026

Cite this article as: Larrieu, T., Grieco, F., Carron, C. *et al.* Inhibition of stress resilience and adult hippocampal neurogenesis by platelet-derived LPA16:0 in anxiety. *Nat Commun* (2026). <https://doi.org/10.1038/s41467-026-69240-3>

Thomas Larrieu, Fabio Grieco, Charline Carron, Marta Vilademunt, Crystal Weber, Kyllian Ginggen, Aurélie Delacrétaç, Hector Gallart-Ayala, Mumeko C. Tsuda, Heather A. Cameron, Chin B. Eap, Julijana Ivanisevic, Pierre Magistretti, Evgenia Salta, Giorgia Tosoni, Dilara Ayyildiz, Ludovic Telley, Alexandre Dayer, Camille Piguet & Nicolas Toni

We are providing an unedited version of this manuscript to give early access to its findings. Before final publication, the manuscript will undergo further editing. Please note there may be errors present which affect the content, and all legal disclaimers apply.

If this paper is publishing under a Transparent Peer Review model then Peer Review reports will publish with the final article.

Inhibition of stress resilience and adult hippocampal neurogenesis by platelet-derived LPA16:0 in anxiety.

Authors: Thomas Larrieu^{1*}, Fabio Grieco¹, Charline Carron¹, Marta Vilademunt¹, Crystal Weber¹, Kyllian Ginggen¹, Aurélie Delacrétaz¹, Hector Gallart-Ayala², Mumeko C. Tsuda³, Heather A. Cameron³, Chin B. Eap^{1,4,5,6}, Julijana Ivanisevic², Pierre Magistretti^{7,1}, Evgenia Salta⁸, Giorgia Tosoni⁸, Dilara Ayyildiz⁸, Ludovic Telley⁹, Alexandre Dayer^{10†}, Camille Piguet¹⁰, Nicolas Toni^{1*}

Affiliations:

¹ Center for Psychiatric Neuroscience, Department of Psychiatry, Lausanne University Hospital, University of Lausanne; Prilly, Switzerland.

² Metabolomics Platform, Faculty of Biology and Medicine, University of Lausanne; Lausanne, Switzerland.

³ Section on Neuroplasticity, National Institute of Mental Health, National Institutes of Health; Bethesda, MD, USA.

⁴ School of Pharmaceutical Sciences, University of Geneva; Geneva, Switzerland.

⁵ Center for Research and Innovation in Clinical Pharmaceutical Sciences, University of Lausanne; Lausanne, Switzerland.

⁶ Institute of Pharmaceutical Sciences of Western Switzerland, University of Geneva; Geneva, Switzerland.

⁷ King Abdullah University of Science and Technology (KAUST); Jenna, Saudi Arabia.

⁸ Laboratory of Neurogenesis and Neurodegeneration, Netherlands Institute for Neuroscience, 1105 BA, Amsterdam, the Netherlands.

⁹ University Claude Bernard Lyon 1, MeLiS—UCBL—CNRS UMR 5284—INSERM U1314, Lyon, France.

¹⁰ Department of Psychiatry, Faculty of Medicine, University of Geneva; Department of Mental Health and Psychiatry, Geneva University Hospital; Geneva, Switzerland.

† Deceased.

*Corresponding author

Prof. Nicolas Toni nicolas.toni@unil.ch
Center for Psychiatric Neurosciences,
Lausanne University Hospital – CHUV
Route de Cery
1008 Prilly-Lausanne, Switzerland
+4121-314-3916

Dr. Thomas Larrieu thomas.larrieu@chuv.ch

Center for Psychiatric Neurosciences,
Lausanne University Hospital – CHUV
Route de Cery
1008 Prilly-Lausanne, Switzerland
+4121-314-6807

Abstract

Anxiety is an aggravating comorbidity of many psychiatric disorders that is often underdiagnosed and undertreated, and little is known on the mechanisms underlying its regulation. Here, we find that serum LPA16:0 abundance increases with trait anxiety in both humans and mice; while high LPA16:0 levels are sufficient to reduce the *in vitro* proliferation of adult hippocampal neural stem/progenitor cells. In humans, the main LPA receptor LPA₁, bears single nucleotide polymorphism variants associated with anxiety. In mice, LPA16:0 decreases hippocampal neurogenesis and stress resilience, whereas LPA₁ antagonism or the reduction of platelets, the main source of circulating LPA16:0, increases adult neurogenesis and resilience to acute stress. Conditional knockdown of LPA₁ receptor in neural stem cells is sufficient to enhance cell proliferation in the dentate gyrus. Finally, the inhibition of adult neurogenesis abolishes the beneficial effect of LPA₁ antagonism on resilience against both acute and chronic stress. Together, these findings identify circulating LPA16:0 as a biomarker of trait anxiety and LPA16:0-LPA₁ signaling as a regulation mechanism of mood-related behavior through the decrease of adult neurogenesis.

Introduction

Anxiety disorders represent the most prevalent forms of mental illnesses, affecting 20-30% of the population aged 15-25 years¹. Their high chronicity and prevalence contribute to their substantial impact on global health, accounting for approximately 3% of the overall disease burden². Moreover, anxiety frequently co-occurs with various psychiatric conditions, exacerbating their severity and increasing the risk of recurrence or relapse^{3, 4, 5, 6}. Unfortunately, anxiety often goes untreated, leading to prolonged suffering for individuals and a persistent burden on healthcare systems^{7, 8, 9}. Thus, to gain a deeper understanding of the underlying mechanisms driving anxiety and its interplay with other psychiatric disorders, adopting a trans-diagnostic framework that incorporates anxiety as a fundamental dimension is crucial.

Individuals diagnosed with anxiety disorders often exhibit heightened reactivity to stress¹⁰, which involves alterations in brain plasticity^{11, 12}, in particular impacting adult hippocampal neurogenesis¹³. Adult neurogenesis results in the continuous generation of new neurons in the adult brain, a process observed in the dentate gyrus (DG) of the hippocampus¹⁴. Interestingly, adult neurogenesis is highly sensitive to changes in lifestyle conditions such as social isolation¹⁵, inflammation^{16, 17} or chronic stress^{17, 18, 19, 20}, all of which are associated with decreased neurogenesis and emotional deficits^{11, 16, 21}. Conversely, the production of new granule neurons is crucial for regulating mood^{18, 22, 23}, promoting stress resilience^{24, 25, 26}, and mediating the effects of antidepressant treatments^{18, 27} whereas increasing adult neurogenesis can produce antidepressant effects²⁸. Thus, adult neurogenesis is both a target of anxiety and stress-related disorders as well as a mediator of stress resilience. However, the mechanisms underlying the effect of anxiety on stress vulnerability and adult neurogenesis are not fully understood. Mechanistically, most of the effects of external factors on adult neurogenesis are mediated by the close cellular environment of adult neural stem/progenitor cells (aNPC), named the neurogenic niche, which includes neurons, astrocytes, oligodendrocytes, microglia, as well as blood vessels. The concept of the vascular neurogenic niche was initially based on observations of the proximity between hippocampal stem/progenitor cells and blood vasculature²⁹ where capillaries serve as a scaffold for progenitor cells' migration³⁰. Ultrastructural observations further showed that hippocampal radial glia-like stem cells form perivascular endfeet at sites of increased capillaries permeability^{31, 32}, suggesting that blood-circulating molecules may directly interact with stem cells and regulate their proliferation and fate despite poor blood-brain barrier (BBB) permeability. In support of this possibility, several studies have uncovered several blood-borne molecules that regulate adult neurogenesis in age-related cognitive impairment or voluntary exercise^{33, 34, 35, 36, 37},

³⁸. However, the role of blood-circulating molecules in the regulation of adult neurogenesis in the context of stress and anxiety is poorly known.

In this work, we use a combination of biochemical approaches, histology and behavioral tests to show that in anxious individuals, platelets produce LPA16:0 that inhibits adult hippocampal stem cell proliferation, leading to decreased neurogenesis and stress resilience.

Results

Serum from anxious mice reduces aNPC proliferation.

To investigate blood-circulating molecules influencing adult hippocampal neurogenesis in anxiety, we developed an *in vitro* model exposing aNPCs to serum from adult male mice. aNPCs were cultured with serum for 24 hours (adherent conditions) or 72 hours (floating conditions), and proliferation was assessed via bromodeoxyuridine (BrdU) incorporation or neurosphere formation (Fig. 1a). Increasing serum concentrations reduced proliferation (Fig. 1b-e); however, 0.2% serum showed no significant effect and was therefore kept for subsequent experiments in adherent conditions. We named this assay the blood-brain axis (BBA) assay. The BBA assay was applied to serum from stress-free (i.e., not subjected to experimental stress) inbred mice exhibiting natural variability in anxiety-related behavior^{39,40}. Trait anxiety was assessed using an elevated plus maze (EPM) and a light / dark test (LDT)³⁹ (Fig. 1f, g and Supplementary Fig. 1), and mice were divided into low-anxiety (LA) and high-anxiety (HA) groups based on the median of their anxiety score (Fig. 1h-i). Eight days post-testing, serum was collected and analyzed in the BBA assay. aNPC proliferation was significantly lower with HA serum than LA serum (Fig. 1j), correlating inversely with trait-anxiety scores (Fig. 1k). This experiment was repeated using a separate group of naïve mice, which confirmed a 15% proliferation decrease with HA compared to LA serum (LA: $100 \pm 4.57\%$, $n=11$; HA: $84.87 \pm 4.67\%$, $n=9$; $p=0.034$). Glucocorticoids exert a bimodal, dose-dependent effect on aNPC proliferation *in vitro*⁴¹. However, corticosterone (CORT) levels showed no differences or correlation with proliferation (Fig. 1l, m). Indicators of apoptosis, including nuclear condensation and caspase-3 activation⁴², revealed no toxicity from HA serum (Supplementary Fig. 2a-d). *In vivo*, BrdU labeling showed reduced cell numbers in the DG of HA mice, correlating negatively with anxiety (Supplementary Fig. 3a, b). DCX staining, though slightly reduced in HA mice, showed no significant differences or correlation (Supplementary Fig. 3c, d).

The BBA assay identifies stress-resilient individuals.

Trait anxiety is defined as an enduring, stable predisposition to experience anxiety across a variety of conditions whereas state anxiety fluctuates and is measured in response to exposure to an anxiogenic context⁴³. To evaluate the BBA assay in state anxiety induced by chronic restraint stress (CRS), mice underwent a 21-day CRS protocol, which induces anxiety- and depression-like behaviors (Fig. 1n)^{11, 44, 45}. After confirming increased state-anxiety scores, elevated serum CORT levels, and absence of weight gain in CRS-treated mice (Fig. 1o-q and Supplementary Fig. 4), sera were collected for analysis in the BBA assay. Serum from CRS-treated mice significantly reduced aNPC proliferation compared to non-stressed controls (Fig. 1r). Replication in an independent cohort confirmed a 14% reduction in aNPC proliferation (CTRL: $100 \pm 4.36\%$, $n=11$; CRS: $86.02 \pm 4.53\%$, $n=11$; $p=0.037$), with proliferation inversely correlating with state-anxiety scores (Fig. 1s). Dividing CRS mice by the median value of proliferation levels revealed that only low-proliferative mice exhibited high anxiety scores (Fig. 1t-u) while dividing mice by anxiety levels showed reduced proliferation only in the high-anxiety group, suggesting that the BBA assay discriminated susceptible from resilient animals (Fig. 1v-w). Consistently, Receiver Operating Characteristic (ROC) analysis demonstrated that the BBA assay achieved 87% accuracy in distinguishing control- from CRS-treated animals (Fig. 1x). Despite elevated free-CORT in CRS-treated mice, no correlation was found between CORT levels and aNPC proliferation (Fig. 1y). Cytotoxicity was also excluded, as serum from CRS-treated mice did not induce nuclear condensation or caspase-3 activation in aNPCs (Supplementary Fig. 2e-h). Together, these results indicate that blood-circulating molecules regulate aNPC proliferation in the context of basal (trait) anxiety and in state-anxiety induced by experimental stress.

Serum from anxious patients reduces aNPC proliferation.

To evaluate the applicability of the BBA assay for human serum, we tested serum from five healthy controls. A 0.2% serum concentration did not affect aNPC proliferation compared to mouse serum (Mouse serum: $35.16 \pm 1.49\%$, $n=11$; Human serum: $38.30 \pm 0.88\%$, $n=5$; $p=0.20$), confirming the BBA assay compatibility. We then examined serum from individuals in the BipOff cohort which consists in young adults with at least one parent diagnosed with a neuropsychiatric disorder linked to emotional dysregulation (e.g., ADHD, BPD, or BD), increasing their risk of developing a psychiatric disorder^{46, 47, 48, 49, 50, 51, 52}. At the time of blood collection, participants underwent structured clinical interviews and were subsequently stratified into two high-risk (HR) subgroups: HR-susceptible, comprising individuals with a confirmed diagnosis of a neuropsychiatric disorder, and HR-resilient, without neuropsychiatric diagnosis (Fig. 2a, b). HR-susceptible individuals exhibited higher trait- and state-anxiety scores compared to HR-resilient and healthy controls (Fig.

2c, d). Furthermore, serum from HR-susceptible individuals significantly reduced aNPC proliferation in the BBA assay, unlike serum from HR-resilient or healthy controls, which had similar effects (Fig. 2e, f). ROC analysis revealed 70% accuracy for cell proliferation in the BBA assay in distinguishing HR-susceptible individuals from controls (Fig. 2g). Cell proliferation inversely correlated with both anxiety measures, with greater reductions linked to higher trait- and state-anxiety scores (Fig. 2h, i) and did not correlate with serum cortisol ($r^2=0.038$, $p=0.28$). Serum from HR individuals also did not impact cell viability, ruling out cytotoxicity (Supplementary Fig. 5a, b).

LPA16:0-LPA₁ signaling is involved in anxiety in patients and aNPC proliferation

To identify molecules mediating the effect of serum on aNPC proliferation in the BBA assay, we performed untargeted metabolomic analysis. Before correction for multiple comparison, three metabolites significantly correlated with aNPC proliferation as well as with anxiety in HR individuals ($p<0.01$): lysophosphatidic acid 16:0 (known as 1-palmitoyl-GPA (16:0) or LPA16:0), fibrinopeptide B, and lysophosphatidylserine 18:0 (known as 1-stearoyl-GPS (18:0), Supplementary data). Among these, LPA16:0 was also elevated in HR-susceptible individuals compared to controls and HR-resilient individuals (Fig. 2j-l). Additionally, LPA16:0 levels correlated with both trait- and state-anxiety in HR individuals (Fig. 2m, n). Of all analyzed LPA forms (14:0, 16:0, 16:1, 16:3, 18:0, 18:1, 18:2, 18:3, 20:4), only LPA16:0 and LPA20:4 were detected in the serum. LPA synthesis primarily involves phospholipase A (PLA1 or PLA2) cleaving membrane phosphatidylcholine (PC) into lysophosphatidylcholine (LPC), followed by autotaxin (ATX) converting LPC into LPA^{53, 54, 55} which can be further converted to diacylglycerol (DAG) by lipid phosphate phosphatase 1 (LPP1, Fig. 2j). HR-susceptible individuals exhibited lower LPC (Fig. 2p) and DAG (Fig. 2q) but unchanged PC levels (Fig. 2o) and displayed increased LPA:LPC ratios (Fig. 2r) without affecting DAG:LPA ratios (Fig. 2s), suggesting that elevated ATX activity contributed to LPA16:0 production in these individuals.

Of the 6 LPA receptors, LPA₁, LPA₂, LPA₄ and LPA₆ are expressed in the hippocampus, with LPA₁ predominantly in adult neural stem cells^{56, 57}. Using the BBA assay, we tested the LPA₁ antagonist Ki16425 and found that it normalized aNPC proliferation when added to HR-susceptible serum (Fig. 2t). Inversely, a non-hydrolysable cyclic form of LPA16:0 (cLPA16:0) or LPA16:0 dose-dependently inhibited aNPC proliferation (Fig. 2u, Supplementary Fig. 5c, respectively). In contrast, LPA18:1 increased aNPC proliferation as previously observed⁵⁷, an effect blocked by an LPA1/LPA3 antagonist diacylglycerol-phosphate (DGPP, Supplementary Fig. 5d). Thus, LPA16:0-

LPA₁ signaling was both necessary and sufficient to explain the effect of serum from HR-susceptible patients on aNPC proliferation in the BBA assay.

To assess LPA₁ gene expression in the hippocampus, we first employed a single-cell transcriptomics dataset of adult mouse dentate gyrus with broad cell types, including cells of the neurogenic trajectory⁵⁸ (Fig. 2v). We observed that the *Lpar1* gene is predominantly expressed in mature oligodendrocytes and adult neural stem cells (RGL) (Fig. 2w-y). Negligible expression levels were also found in ependymal cells which originate from the same embryonic progenitor as neural stem cells⁵⁹. To probe the relevance of these observations to the human brain, we used a recently generated single-nucleus RNA-sequencing dataset from postmortem human dentate gyrus⁶⁰, from which we extracted data on individuals aged 20 years and older. Similarly to the mouse hippocampus, *LPAR1* was primarily expressed in adult human oligodendrocytes and to a lesser extent in microglia. When examining the neurogenic lineage, we found *LPAR1* expression in neuroblasts, intermediate progenitors and stem cells (Fig. 2z-γ). Finally, we analyzed an in-house dataset that focused on adult human immature neurons⁶¹, in which we found *LPAR1* expression in several subpopulations of immature neurons (Supplementary Fig. 5e-h).

Using the GeneAtlas UK Biobank⁶² and the PsyMetab cohort (2479 patients), we examined genetic associations between anxiety and single nucleotide polymorphisms (SNPs) on the genes involved in LPA signaling (LCAT, PLA1A, ENPP2, PLPP1, and LPAR1). We found that the rs10817103C>T SNP in LPAR1 was associated with reduced anxiety risk (odds ratio: 0.61, 95% confidence interval: 0.43-0.86, p=0.005) and decreased LPA₁ expression⁶³. Together, this genetic analysis supports our experimental results showing that LPA16:0-LPA₁ signaling is involved in anxiety in humans.

The regulation of stress resilience by LPA16:0-LPA₁ signaling requires adult neurogenesis

To investigate the role of LPA16:0-LPA₁ signaling in anxiety and stress responses, we first measured LPA16:0 levels in mouse serum. Trait anxiety was assessed in naïve mice using an EPM and LDT, classifying them as low-anxiety (LA) or high-anxiety (HA) groups (Fig. 3a, b and Supplementary Fig. 6a-f). Targeted metabolomic analysis revealed significantly elevated serum concentrations of LPA16:0, LPA20:4, and LPA18:2 in HA mice compared to LA mice, with no changes in LPA18:0 or LPA18:1 (Fig. 3c and Supplementary Fig. 6g-j). LPA16:0 concentration positively correlated with individual anxiety scores (Fig. 3d) and accurately identified HA mice with 80% accuracy (Fig. 3e), suggesting that LPA16:0 had a similar role in mice anxiety as in humans. To assess the long-term persistence of trait anxiety phenotypes, we tested an independent cohort of naïve mice. We found that individuals that were identified as HA still displayed increased anxiety

6 weeks after their initial assessment (Fig. 3f, g and Supplementary Fig. 7). This behavioral profile was accompanied by reduced hippocampal stem cell proliferation (Ki67⁺ cells) and reduced survival of newborn neurons (IdU⁺ cells), labeled six weeks prior to sacrifice (Fig. 3h, i). These findings suggest that elevated trait anxiety is a persistent trait that is associated with reduced adult hippocampal neurogenesis and elevated serum LPA16:0 levels. To evaluate the effects of exogenous LPA16:0 on anxiety and neurogenesis, anxiety-matched mice were treated with cyclic LPA16:0 (cLPA16:0) or vehicle daily for 21 days. Behavior, serum, and brain samples were analyzed post-treatment (Fig. 3j). cLPA16:0-treated mice displayed no baseline anxiety changes compared to vehicle-treated mice (Fig. 3k and Supplementary Fig. 8a-c). However, after exposure to 20 minutes of acute restraint stress (ARS), a paradigm known to reveal susceptible phenotypes by reducing stress reactivity thresholds^{64, 65}, cLPA16:0-treated mice showed heightened anxiety-like behavior (Fig. 3k right and Supplementary Fig. 8d, e), indicating that LPA16:0 may exacerbate stress response. In addition, cLPA16:0-treated mice displayed reduced Ki-67-positive cell proliferation in the DG (Fig. 3l, t), and their serum decreased aNPC proliferation in the BBA assay compared to vehicle-treated mice (Fig. 3m). A negative correlation between serum LPA16:0 levels and aNPC proliferation in the BBA assay further supported its impact on neurogenesis (Fig. 3n). Although the LPA₁ receptor expression in the hippocampus is predominant in stem cells, the transcriptomics data suggests that oligodendrocytes and microglia may participate to the effect of cLPA16:0 on neurogenesis and anxiety. To assess the effect of chronic cLPA16:0 administration on these 2 cell populations, we quantified the density of microglia, mature oligodendrocytes and oligodendrocytes precursor cells, in these mice (Supplementary Fig. 9). We found no significant difference in the density and proliferation of these cell types between vehicle- and cLPA16:0-treated mice, suggesting that cLPA16:0 did not induce changes in these cell populations. To determine whether LPA₁ antagonism enhances stress resilience, anxiety-matched mice were treated with Ki16425 or vehicle for 12 days before undergoing 6 hours of ARS (Fig. 3o). Ki16425 did not modify baseline anxiety, but increased stress resilience (Fig. 3p and Supplementary Fig. 10a-e). Resilience was associated with increased aNPC proliferation (Fig. 3q, u) and enhanced expression of DCX in the DG (Fig. 3r, v). These effects were replicated in a separate experiment in a different laboratory in the USA (Fig. 3s and Supplementary Fig. 10f-j), confirming that antagonizing LPA₁ increases adult neurogenesis and resilience to an acute stress. To assess whether reducing LPA₁ receptor activity on hippocampal stem cells was sufficient to increase cell proliferation, we generated a mouse model that enables the conditional knock-down of the LPA₁ receptor specifically in stem cells. To this aim, we crossed the tamoxifen-inducible Gli1-CreEr^{T2}:tdTomato mouse⁶⁶ with the flanked LPAR1^{fl/fl} mouse⁶⁷. Five days after tamoxifen injection,

Gli1-LPA1^{+/-} mice displayed an increase in cell proliferation as compared to Gli1-LPA^{+/+} control mice. These results mimic the effect of LPA₁ antagonism, supporting the view that reduced LPA₁ activity in adult hippocampal stem-progenitor cells is sufficient to increase their proliferation. To investigate whether the effect of Ki16425 on resilience was dependent on adult neurogenesis, naïve mice were pretreated with the anti-mitotic drug temozolomide (TMZ) on the first 3 days of each week for 4 weeks to suppress neurogenesis. After 3 weeks of TMZ or NaCl treatment, mice underwent Ki16425 administration for 12 days and were assessed for resilience to a 6h-ARS (Fig. 3y). While Ki16425+NaCl-treated mice displayed resilience to 6h-ARS, Ki16425+TMZ-treated mice exhibited heightened anxiety (Fig. 3z and Supplementary Fig. 11) and reduced DG cell proliferation (Fig. 3α).

To examine the effect of Ki16425 on depressive-like behavior under chronic stress conditions, anxiety-matched mice were treated with NaCl or TMZ for the first 3 days of each week for 4 weeks and subjected to 21 days of CRS. Mice were injected daily with Ki16425 or vehicle for 25 days 4 days before CRS. After 2 days of CRS regimen, mice received 3 injections of BrdU every 2 hours. Mice were then assessed for anxiety (MBT) and depression-like behavior (NSFT; Fig. 3β). No anxiety differences were detected in the MBT (Fig. 3γ), but Ki16425-treated mice exhibited reduced feeding latency in a NSFT, indicating reduced depression-like symptoms as compared to vehicle-treated mice (Fig. 3δ). This effect was abolished by TMZ treatment, highlighting the requirement of neurogenesis for Ki16425's action. Consistently, the Ki16425-mediated increase in cell proliferation (Fig. 3ε) and in the number of newly formed neurons (Fig. 3ζ) in the DG was blocked by TMZ treatment. Together, these results indicate that the increase in adult neurogenesis was required for the antidepressant effect of Ki16425 after stress.

Platelet depletion reduces circulating LPA16:0, increases stress resilience and adult neurogenesis.

Serum LPA is primarily produced by platelets^{68, 69, 70, 71}, with thrombocytopenia significantly reducing circulating LPA^{71, 72}. To evaluate whether reducing platelets lowers LPA16:0, 4 mice were injected with anti-platelet or control serum for two days and their plasma was pooled. Plasma analysis showed that anti-platelet treatment eliminated platelets and reduced LPA16:0 to undetectable levels (Fig. 4a). Next, we tested the effect of platelet depletion on neurogenesis and stress resilience. Anxiety-matched mice received anti-platelet serum every two days for 20 days^{73, 74} and were tested in an OFT followed by a 6-hour ARS (Fig. 4b). Platelet-depleted mice exhibited reduced baseline anxiety and resilience to ARS compared to controls (Fig. 4c and Supplementary Fig. 12). This resilience profile was associated with increased aNPC proliferation in the DG (Fig.

4d), demonstrating that platelet depletion mimics the stress-resilience effects of LPA₁ antagonism by eliminating circulating LPA16:0.

Discussion

In the present study, we found that spontaneously anxious mice exhibited reduced cell proliferation and adult neurogenesis in the dentate gyrus of the hippocampus. Using an *in vitro* model of adult neurogenesis, the BBA assay, we observed that serum from spontaneously anxious mice, experimentally stressed mice or human patients suffering from anxiety, reduced aNPC proliferation proportionally to their anxiety levels. Untargeted mass spectrometry identified that the serum concentration of LPA16:0, a signaling lipid, correlated with anxiety in humans and mice as well as with the effect of their serum on aNPC proliferation *in vitro*. LPA16:0 was necessary and sufficient to replicate the effect of human serum on the BBA assay, which was mediated by the LPA₁ receptor. In a combined analysis of the GeneAtlas and an in-house cohort of patients, we found an association between anxiety and the rs10817103C>T SNP on the enhancer region of the *LPAR1* gene, which is known to decrease LPA₁ expression. Furthermore, LPA16:0-LPA₁ signaling in mice bidirectionally regulated stress resilience and adult neurogenesis and the increase in stress resilience produced by LPA₁ antagonism was mediated by adult neurogenesis. The increase in cell proliferation following LPA₁ antagonism was mimicked by the hippocampal stem cells-specific knock-down of this receptor. Finally, the depletion of platelets, the main source of LPA in blood, reduced LPA16:0 and induced stress resilience along with increasing aNPC proliferation in the dentate gyrus. Together, these results highlight a crucial role of platelets in stress susceptibility in anxious individuals, mediated by the production of LPA16:0 and the inhibition of adult hippocampal neurogenesis.

Growing evidence indicate that blood-circulating molecules regulate brain plasticity, as demonstrated by blood transfusions or parabiosis experiments^{33, 34, 35, 37, 38, 52}. To circumvent the technical limitations of these experiments, we have developed a simple *in vitro* model of adult hippocampal neurogenesis, named the BBA assay, that enables the discovery of blood-circulating molecules that regulate adult hippocampal neurogenesis in mice. The BBA assay exploits the sensitivity of aNPC to molecular signaling in the neurogenic niche that is enabled by the extended repertoire of membrane receptors they express⁷⁵. Due to the difficulty of assessing adult neurogenesis in humans^{76, 77, 78, 79, 80, 81}, the relevance of the BBA assay for human adult hippocampal neurogenesis was not addressed here. However, the observation of LPA₁ reporter mice⁵⁷ and single cell gene expression data on mice and humans indicates LPA₁ expression in niche cells and stem cells. Thus, the shared repertoire of receptors between aNPC and niche

cells supports the use of the BBA assay as a cell-based biomarker of the integrity of the hippocampal neurogenic niche, which is relevant to its role in emotional regulation and stress resilience. The present study highlights the translational value of the BBA assay which, combined with untargeted metabolomics and clinical assessment, provides an entry point for the identification of novel mechanisms of regulation of adult neurogenesis by circulating molecules in the context of anxiety disorders. Similar approaches have been used to study the role of circulating molecules in other diseases related to hippocampal dysfunction such as Alzheimer's disease^{82, 83} or depression⁸⁴.

The different forms of LPA play a role in several cellular processes that include smooth muscle contraction⁸⁵, platelet aggregation⁸⁶, cell growth and differentiation⁸⁷, inflammation⁸⁸ and emotional regulation^{89, 90, 91}. While most research focuses predominantly on LPA18:1, the role of the distinct LPA16:0 species in brain function and stress resilience remains unexplored. The main source of LPA in the blood are platelets^{68, 69, 70, 71, 72}. Although platelets are principally known for their role in clot formation, they also interact with brain cells^{92, 93}, in particular in pathological contexts^{94, 95}, where they promote functional recovery⁹⁶. Upon activation, platelets can release several molecules that play an important role in neuronal function, such as neurotransmitters-neuromodulators^{97, 98} or brain-derived neurotrophic factor (BDNF)⁹⁹ and LPA16:0 is one of the most increased lipids in activated human platelets⁶⁹. Interestingly, several psychiatric diseases are associated with increased platelet activation^{100, 101}, which may underlie the increased production of LPA16:0 in anxious individuals observed here.

Notably, platelets also release molecules that promote adult hippocampal neurogenesis^{74, 102}. In particular, platelet factor 4 (PF4) production is stimulated by physical exercise and mediate the stimulating effect of physical exercise on adult hippocampal neurogenesis⁷⁴. It is unclear how these different signaling pathways contribute to the net effect on adult neurogenesis, especially after platelet depletion, which reduces both circulating LPA16:0 (Fig. 4) and PF4¹⁰³. Future investigations comparing platelets secretome may shed light on the effect of different stimulating conditions on platelet activation and neurogenesis regulation. Furthermore, the effect of these molecules may be altered by the disease state. Indeed, in physiological conditions, LPA is produced in the extracellular space from cell membrane phospholipids by the soluble enzyme autotaxin. In return, LPA inhibits autotaxin, leading to a negative-feedback loop that enables LPA homeostasis⁵³. In the context of inflammation, inflammatory cytokines disrupt this feedback regulation, leading to increased LPA production^{88, 104}. Inflammation is elevated in anxiety and mood disorder patients^{105, 106, 107, 108} and thus, LPA feedback dysregulation together with SNPs on genes for LPA₁ may contribute to increased LPA-LPA₁ signaling in patients with anxiety. In turn,

by increasing anxiety after a moderate stress, LPA16:0 may contribute to maintaining an anxious state. Therefore, the overall impact of platelet depletion on adult neurogenesis likely reflects the specific physiological or pathological context in which platelet activation occurred in the first place. However, the interplay between these distinct signaling pathways remains poorly understood, and further mechanistic studies are warranted to delineate their respective contributions to the regulation of adult neurogenesis and stress resilience.

Together, the experimental evidence presented here suggests that platelets in anxious individuals produce circulating LPA16:0 that target the LPA₁ receptor, leading to reduced adult neurogenesis and impaired stress resilience. This mechanism may contribute to the pathophysiology of many psychiatric conditions and offer novel therapeutic avenues. Finally, the BBA assay presented here, together with serum LPA16:0 measurements may provide a diagnostic tool to assess anxiety in psychiatric patients, paving the way for personalized treatment.

Methods

The blood-brain axis (BBA) assay

Cell culture: The adult neural stem/progenitor cell line (aNPC) is a kind gift from the laboratory of Fred Gage (Salk Institute, San Diego, USA). They were originally isolated from the dentate gyrus DG of 8-week-old adult Fisher 344 rats and cultured in medium Dulbecco's Modified Eagle Medium (DMEM/F12) supplemented with N2 and FGF-2 (20ng/ml) as previously described¹⁰⁹. The stem/progenitor identity of these cells was confirmed by immunostaining indicating that 90% of these cells expressed Tbr2, 97% expressed Nestin and 99% expressed SOX-2 (data not shown and¹¹⁰). aNPCs were plated at a density of 60,000 cells per well (total volume = 500µl) in a 24-well-plate coated with Poly-D-lysine hydrobromide at 0.1mg/ml (P6407 sigma-aldrich) and Laminin at 20µg/ml (23017015 Life technologies). Twenty-four hours after plating, the medium was removed and replaced with fresh medium containing 0.2% serum for 24h. The medium was then supplemented with 5 µM BrdU for 30 min and washed twice with pre-heated fresh medium and fixed with 4% paraformaldehyde for 30 min. The plate was briefly washed with PBS 0.1M and stored at 4°C until used. Immunocytochemistry against BrdU and/or Ki-67 was processed as follows: BrdU immunohistochemistry was preceded by DNA denaturation with 2 M HCl for 15 min at 37°C, and rinsed in 0.1 M borate buffer pH 8.5 for 15 min. Then, aNPC were incubated in blocking solution containing 0.3% Triton-X100 and 10% deactivated horse serum (Gibco, 16050122) for one hour. Plates were incubated at 4°C with mouse monoclonal anti-BrdU (24 h, 1:250, Abcam) or Rabbit anti-Ki-67 (1:300, Abcam, ab15580) followed by goat anti-mouse 488

(1:300, Invitrogen) or goat anti-rabbit 488 (1:300, Invitrogen), respectively for 1 h at room temperature. After immunostaining, 10 minutes incubation into 4,6 diamidino-2-phenylindole (DAPI, 1:500) was used to reveal nuclei.

For neurosphere cultures, aNPC were grown with 0.2% serum at a density 60,000 cells per well in a 24-well-plate under floating conditions and were incubated at 37°C for 3 days. The neurospheres were counted and their size measured using an inverted light microscope and the ImageJ software. Control cultures were treated with serum-free medium.

Image acquisition and analysis for in vitro experiments: Images were acquired using an Eclipse Ti2 inverted microscope (Nikon). The number of BrdU-labeled aNPC was counted in one randomly selected large field (tiles 4x4) in each well of the plate. For the validation of the BBA assay (Fig. 1B), we used 2-3 wells per condition in 3 independent replicates. For all other experiments, each well stands for an experimental unit and was replicated at least twice using 2 independent cohorts of mice for each condition (trait and state conditions). The number of BrdU-labeled aNPC was compared with the total number of aNPC in each selected field to obtain a proliferation ratio, which was then normalized to the control group values to enable comparisons across conditions.

Cell viability: Cell viability was evaluated using the WST-1 assay. Cells (6.0×10^4 cells/well) were grown in 24-well plate. After exposure to serum for 24h., 25 μ l cell proliferation reagent WST-1 (Roche, Cat. No. 05015944001, Switzerland) was added to each 500 μ L/well serum-free DMEM/F12 (0.5:10 dilution), followed by incubation for 2 hours at 37°C. Absorbance was measured at 440 nm using a microplate reader (Tecan, Männedorf, Switzerland).

Mice

All experiments were performed with the approval of the Cantonal Veterinary Authorities (Vaud, Switzerland) and carried out in accordance with the European Communities Council Directive of 24 November 1986 (86/609EEC). All experiments were performed on C57Bl/6J male mice obtained from Janvier Laboratories. After arrival, animals were housed four per cage and allowed to acclimate to the vivarium for one week. All animals were subsequently handled for 1 min. per day for a minimum of 3 days. Animals were weighted upon arrival as well as weekly to monitor health. Gli1-CreEr^{T2}:tdTomato reporter mice⁶⁶ (referred to as Gli1-LPA1^{+/+}) were a kind gift from Prof. Jessberger (University of Zurich) and LPAR1^{ff} mice⁶⁷ were a kind gift from Prof. Jerold Chun (Sanford Burnham Prebys Medical Discovery Institute, La Jolla, CA, USA). These mice were

crossed to generate Gli1-CreEr^{T2}:tdTomato^{+/-} / LPAR1^{+/-} offspring (referred to as Gli1-LPA1^{+/-}). Both Gli1-LPA1^{+/-} and Gli1-LPA1^{+/+} (as controls) mice were administered tamoxifen (70 mg/kg, intraperitoneally) twice in one day. The recombination of the LPAR1 gene in Gli1-LPA1^{+/-} mice resulted in the hemizygous expression of LPAR1 in stem cells and these mice were named Gli1-LPA1^{+/-} (Fig. 3W). Mice were maintained under standard housing conditions on corn cob litter in a temperature- (23 ± 1°C) and humidity- (40%) controlled animal room with a 12h. light/dark cycle (8–20 h.), with unlimited access to food and water.

Chronic and acute restraint stress

This protocol involved 21 days of chronic restraint stress (CRS) as previously described^{44, 111}. Animals were randomly assigned to either the control or CRS group. Animals were introduced headfirst into 50 ml Falcon tubes (11.5 cm in length; diameter of 3 cm) from which the cap was removed, and the bottom was perforated with four 0.4 cm holes to enable breathing. Tissue was added at the caudal extremity to adjust the physical constraint to the mouse size and to allow the tail to expand out of the tube. This setting immobilizes the body of the mouse except the head. The mice were subjected to this restrained environment for two consecutive hours every day for a period of 21 days. Control mice were left undisturbed in their home cage except for handling and body weighting each day for 21 days. The acute restraint stress protocol is based on the protocol as previously described⁶⁵. Animals of the stress group were restrained once, using the protocol described for the chronic stress. After one 20-min-restraining or 6-hours-restraining period, mice were transferred into their home-cage for an additional 20 min interval followed by an open-field test to assess anxiety-like behavior.

Behavioral tests

Open-field test (OFT): The test was performed as previously described^{111, 112}. The apparatus consisted of a square Plexiglas arena (40 x 40 x 40 cm) that was illuminated with dimmed lights (25 lx). The floor was cleaned between each trial to eliminate olfactory cues. Mice were introduced facing the wall of the arena and allowed to freely explore the arena for 10 min. A virtual center zone (15 x 15 cm), thigmotaxis zone (30 x 30 cm) and an intermediate zone were included for the behavioral analysis as indicator for anxiety-like behavior. A video tracking system (Anymaze) recorded the path of each mouse as well as the total distance travelled, and the time spent exploring each zone.

Elevated plus maze test (EPM): The test was performed as previously described¹¹². The apparatus was made from black PVC with a white floor. The apparatus consisted of a central platform (5 x 5 cm) elevated from the ground (65 cm) with two opposing open (30 x 5 cm) and two opposing (30 x 5 x 14 cm) closed arms. Light conditions were maintained at 14–15 lux in the open arms, and 3–4 lux in the closed arms. Animals were placed at the end of the closed arms facing the wall, after which the animals were allowed to freely explore the apparatus for 5 min. Mice were tracked (Anymaze) to measure the time spent in each arm and in the risk zones (edge of the open arms).

Light/Dark Test (LDT): The LDT was performed as previously described⁴⁰. A 60 x 40 x 21 cm high Plexiglas box was divided into a dark (20 x 40 x 21 cm) and a light (40 x 40 x 21 cm; 400 lux) compartments separated by an open door (5 x 5 cm) located in the center of the partition at floor level. Each mouse was placed into the light chamber facing the door. Mice were allowed to freely explore the apparatus for 6 minutes. The Anymaze software was used to analyze anxiety-like behavior by calculating the time spent in each zone.

Marble burying test (MBT): As previously described¹¹³, the apparatus consists of an open transparent plastic box (40 x 25 x 20 cm) filled around 6 cm deep with bedding material across the whole cage. Twenty dark marbles (diameter: 16 mm) are spaced evenly in a 4 x 5 grid on the bedding. Mice were given 20 minutes to freely explore the cage (400 lux). At the end, the mice are removed, and every buried marble (more than 2/3 covered by litter) is counted. The number of buried marbles is used as an indicator of anxiety.

Novelty suppressed feeding test (NSFT): As previously described¹¹⁴. The apparatus consists of a square Plexiglas arena (40 x 40 x 40 cm; > 400 lx). The floor was layered with approximately 2 cm of wood bedding. In the center of the square, a single pellet of food was placed on a white paper circular taped to a tissue culture disk (20 x 100 mm). Twenty-four hours before the test, all the food was removed from the home cage to food restricted the mice. The mice were introduced into the arena, facing the wall, and given 3 minutes for free exploration. Anymaze video tracking system recorded the movement trajectory of each mouse, and the videos were analyzed to assess the latency for the first bite. After the test, the food pellet was removed, and the mice were then returned to their cage with food and the amount of food consumed in 20 minutes was measured (in-cage consumption).

Anxiety scores: The anxiety scores were a simplified version of principal component-based analyses^{115, 116} and encompassed several anxiety tests to obtain a general profile of anxiety, as previously described^{115, 116, 117, 118}. The anxiety score was calculated with the average of standardized scores of each anxiety-related behavior tests. For Fig. 1H, 1Q and 3B, this score included the relative time spent in the dark chamber of the LDT and the relative time spent in the closed arm of the EPM. For Fig. 3F-U and figure 4C, D, this score included the relative time spent in thigmotaxis and in the center of the arena of an open-field. Standardization consisted in subtracting the minimum value of the whole population to the value of each animal and dividing the result by the maximum value of the whole population minus the minimum value of the whole population: $(x - \text{min value}) / (\text{max value} - \text{min value})$. This procedure yields scores which are distributed along a scale from 0 to 1, where 1 reflects high anxiety. To assess anxiety levels in each group, a one-sample t-test was employed, using 0.5 as the hypothetical threshold value as scores were distributed along a scale from 0 to 1. If the mean anxiety score of a group exceeded 0.5, it was classified as anxious; if the score was below 0.5, the group was considered non-anxious. This approach allowed for a statistical comparison of each group's anxiety levels against the predefined baseline of 0.5, facilitating clear distinctions between anxious and non-anxious subjects.

Mouse blood collection and preparation

Blood was collected (Multivette® 600 µl, Clotting Activator/Serum) by intracardiac puncture using a 1ml syringe with a 21G7/8 needle after pentobarbital (10 ml/kg, Sigma-Aldrich, Buchs, Switzerland) anesthesia before mouse perfusion. After sampling, the blood was left undisturbed at room temperature for 15 minutes to enable clotting. The clot was removed by centrifuging at 1,500 x g for 10 minutes in a refrigerated centrifuge. The resulting supernatant (i.e., serum) was transferred into a clean polypropylene tube using a Pasteur pipette. The samples were apportioned into 0.5 ml aliquots and stored at - 80°C.

Preparation of platelet-rich plasma (PRP) after anti-platelet serum injection.

Mice were injected with an antiplatelet serum or a control serum for 2 consecutive days. After pentobarbital (10 ml/kg, Sigma-Aldrich, Buchs, Switzerland) anesthesia, whole blood was collected transcardially using a 21G7/8 needle containing 10% of sodium citrate, then transferred into plastic tubes. The platelet count was measured using 20 µl of whole blood in a Sysmex XE-2100™ automated hematology system. Blood samples were centrifuged at 1900 g for 1 minute with no brake at room temperature. The plasma and buffy coat were collected as PRP into a new

tube. PRP was stored at -20°C for 15 min to activate platelets. Samples were then used for targeted LPA16:0 quantifications. The platelet counts and LPA16:0 levels were determined from a pool of 4 mice per condition, i.e., control serum- and antiplatelet serum-treated groups.

Corticosterone measurement

Serum (6 μL) was prepared according to manufacturer's instructions to measure free corticosterone concentrations using an ELISA kit (Enzo Life Sciences, ADI-901-097). The method plots the standards versus hormone concentrations using linear (y) and log (x) axes and performs a 4-parameter logistic fit. Concentration of samples were then calculated from the fit.

BrdU and IdU administration

Mice were injected intraperitoneally with 5-bromo-2-deoxyuridine (Sigma-Aldrich, Buchs, Switzerland) at a concentration of 100 mg/kg in saline (final dilution at 10 mg/ml), 3 times per day at 2-h. intervals in a single day. For proliferation studies, mice were sacrificed 24 hours after the last BrdU injection. To assess the basal level of adult hippocampal neurogenesis in HA vs LA individuals, IdU (57.5 mg/kg; 10 mg/ml) was dissolved in a 0.2 NaOH/saline solution and injected i.p., three times the same day, starting from 11 am with 2 h interval between each injection. For survival study, mice were sacrificed 6 weeks after the last IdU injection.

Tissue collection and preparation

Mice received a lethal dose of pentobarbital (10 ml/kg, Sigma-Aldrich, Buchs, Switzerland) and were perfusion-fixed with 50 ml of 0.9% saline followed by 50 ml of 4% paraformaldehyde (Sigma-Aldrich, Switzerland) dissolved in phosphate buffer saline (PBS 0.1 M, pH 7.4). Brains were then collected, post-fixed overnight at 4°C , cryoprotected 72h in 30% sucrose and slowly frozen on dry ice. Coronal frozen sections of a thickness of 40 μm . were cut with a microtome-cryostat (Leica MC 3050S) and slices were kept in cryoprotectant (30% ethylene glycol and 25% glycerin in $1\times$ PBS) at -20°C until being processed for immunohistochemistry.

Brain slices immunohistochemistry

Immunochemistry was performed as previously described¹¹⁹. For BrdU/NeuN immunostaining, sections were washed 3 times in PBS 0.1M. BrdU detection required formic acid pre-treatment (formamide 50% in $2\times$ SSC buffer; $2\times$ SSC is 0.3M NaCl and 0.03 M sodium citrate, pH 7.0) at 65°C for 2 h followed by DNA denaturation for 30 min in 2 M HCl for 30 min at 37°C and rinsed in 0.1 M borate buffer pH 8.5 for 10 min. Then, slices were incubated in blocking solution

containing 0.3% Triton-X100 and 10% deactivated horse serum (Gibco, 16050122) for 1 h. After blocking, samples were incubated with primary antibodies, at 4°C overnight and then incubated with secondary antibodies for 1 h. For Ki67 and DCX immunostaining, slices were incubated in blocking solution (0.3% TritonX-100 and 10% horse serum in PBS) at room temperature for 1 h and then incubated under agitation at 4° C overnight in a blocking solution containing primary antibodies. After being washed again in PBS, sections were incubated for 2 hours in secondary antibodies. After immunostaining, slices were incubated for 10 min into DAPI (1:500) to reveal nuclei. Sections were mounted onto glass slides and cover-slipped using FluorSave (Millipore). One out of 6 sections (for a total of 10 sections) were imaged using a Nikon NI-E spinning disk fluorescence microscope.

For BrdU and Ki67 immunostaining analyses, we counted the total number of immunostained cells in the DG in the entire thickness of the sections in a 1-in-6 series of section, for a total of 10 sections, with a 40× objective. The average number of cells was then multiplied by 60 to estimate the total number of immunolabeled cells per DG. For DCX analysis, we assessed the proportion of immunostained pixels on each image. Data is expressed either as pixels/area (i.e. region of interest, Supplementary Fig. 3), or fractional volume (Fig. 3r). For the pixels/area analysis, images were acquired using a digital camera (3CCD Hitachi HV-F202SCL) on a slide scanner microscope (×20 objective, Zeiss axioscan Z1). The number of DCX-immunostained pixels was quantified in similar regions of interest, in arbitrary units as the mean of all isolated pixels of soma. Each optical density was normalized by the subtraction of a slide section in which signal was absent (black) using image analysis software Zen 2 (black 8.0 edition and blue 2012 edition). The area of the DG was also measured using Zen blue edition software and no change in DG area was found between groups (data not shown). For the fractional volume analysis of DCX staining (Fig. 3r), images were acquired using a Nikon NI-E spinning disk fluorescence microscope of similar regions of interest between slices. We calculated the fraction of the total volume that is occupied by a DCX-positive signal in each section. The mean fractional volume per animal was derived from the average values of all sections analyzed. For Olig2 and Iba1 immunostaining analyses, images of the entire dentate gyrus were acquired using the same Nikon NI-E spinning disk microscope. ROIs encompassing the hilus, GCL, and molecular layer were defined using Nikon GA3 analysis software (Nikon Instruments Inc., Tokyo, Japan). Automated quantification of Olig2+ and Iba1+ cells was performed within these ROIs. Olig2 and Iba1 cell density was calculated by dividing the number of Iba1+ and Olig2+ cells in the hippocampal region of interest by the sampled volume, defined as the measured hippocampal surface area multiplied by the 40 μm section

thickness. Additionally, for Olig2, the number of double-positive Olig2+/Ki67+ cells was quantified using the colocalization module of the GA3 software.

Reagents and antibodies

For primary antibodies: mouse monoclonal anti-BrdU (1:250, Chemicon International, Dietikon, Switzerland), rabbit anti-DCX (1:500, Cells Signaling Technology, 4604S), rabbit anti-NeuN (1:1000, Abcam, EPR12763), rabbit anti-Ki-67 (1:300, Abcam, ab15580); rabbit anti-cleaved caspase3 (1:500, cell signaling 9579); rabbit anti-Olig2 (1:500, AB9610); Goat anti Iba1 (1:1000, AB5076). For secondary antibodies: goat anti-mouse Alexa-594 (1:300, Invitrogen), goat anti-rabbit 594 (1:300, Invitrogen), and Donkey anti-goat (1:300, A-11058). For drugs: staurosporine (STS, from Cell Signaling Technology, 9953S), cyclic LPA16:0 (0.01 mg/ml in PBS 0.1M and 0.1% BSA fatty acid free, Polar Avanti, 7999268-68-1), DGPP (50 μ M in ddH₂O and 5% ethanol, Polar Avanti, 474943-13-0), Ki16425 (0.5 mg/ml in ddH₂O and 10% ethanol, Cayman Chemical, 10012659), temozolomide (TMZ, from Sigma-Aldrich, T2577, (25 mg/kg; 2.5 mg/ml in 0.9% NaCl i.p.), and rabbit anti-platelet serum (1:2 in PBS, 200 μ l per mouse, Rabbit anti-mouse Thrombocyte; Accurate Chemical & scientific corporation; catalog Number: AIA31440).

Human participants

Participants from the BipOff cohort: The research was conducted according to the principles of the Declaration of Helsinki and approved by the University of Geneva research ethics committee (CER 13-081). All participants gave written informed consent prior to assessment. Offspring of patients were recruited after their parents gave a formal consent to contact their children. We obtained blood samples from 66 individuals from the BipOff cohort of the Geneva University Hospital: 37 offspring at high-risk (HR) of developing a psychiatric disorder, defined as having at least one parent with either ADHD or Borderline Personality Disorder (BPD) or Bipolar Disorder (BD) and 31 healthy control subjects with no history of neuropsychiatric disorder among their parents (CTRL). The offspring were between 15 and 25 years of age at inclusion, and controls between 15 and 30 years old. Control subjects were matched for age, gender, laterality and years of education. Parents were outpatients from the specialized program for BPD/ADHD/BD patients at Geneva University Hospital, where structured diagnostic assessment was conducted. Psychiatric diagnoses in all subjects were established by trained psychologists using the Diagnostic Interview for Genetic Studies (DIGS) or the Kiddie Schedule for Affective Disorders and Schizophrenia (K-SADS) under 18 years of age. This psychiatric assessment led to the stratification of high-risk individuals into two groups; HR-susceptible (n=22) or HR-resilient (n=15),

based on whether they had developed a neuropsychiatric disorder at the time of evaluation. Inclusion criteria were based on age, history of psychiatric or neurological treatment for the subjects and their parents, as assessed during the interview of the subjects. Exclusion criteria for all participants were a history of head injury, current alcohol or drug abuse, daily medication. Assessment of anxiety was conducted through a classical self-report questionnaire, the State-Trait-Anxiety Inventory (STAI)¹²⁰. The STAI is a validated 40-item self-report questionnaire that measures both state (20 items) and trait (20 items) general anxiety. Trait anxiety scores were assessed during the evaluation visit 1-3 weeks prior to lab visit. STAI scores were assessed immediately prior to blood sampling. Blood samples (5ml) were kept on ice for about 1 h and were left for clotting for 30 minutes, followed by centrifugation (5 min at 2300g at room temperature). Samples were then aliquoted and frozen at -20°C for 1-4 hours and then stored at -80°C.

Participants from the PsyMetab cohort: Since 2007, a longitudinal observational pharmacogenetic study (referred to as PsyMetab) approved by the Swiss Association of Research Ethics Committees is ongoing in the Department of Psychiatry of the Lausanne University Hospital. Patients starting a psychotropic treatment associated with a risk of developing metabolic disturbances (i.e., antipsychotics, mood stabilizers or some antidepressants)¹²¹ were included. Clinical data including concomitant medication prescriptions were collected during hospitalization or in outpatient centers during medical examinations based on the department guideline for the metabolic follow-up of psychotropic drugs¹²². In the present study, drug prescription was used to assess anxiety. Patients who were prescribed any benzodiazepine specifically used for treating anxiety symptoms (i.e. alprazolam, bromazepam, clorazepate, ketazolam, lorazepam, oxazepam, prazepam or chlordiazepoxide, as well as clobazam or diazepam if not co-prescribed with any antiepileptic agent) were considered as suffering from anxiety, while other patients were considered as not suffering from anxiety. Two thousand four hundred seventy-nine patients were included in this analysis.

Metabolomics

Non-targeted global metabolomic profiling of serum derived from the BipOff cohort was performed by Metabolon (Durham, NC, USA) as previously described^{123, 124, 125}. Sixty-six experimental samples and 12 Quality Control (QC) samples were analyzed in parallel with the experimental samples in each analysis. The QC samples were generated directly from the experimental samples by taking a small aliquot of each and pooling together. This pool was run as technical replicates during the analysis.

Sample Preparation: Samples were prepared using the automated MicroLab STAR® system from Hamilton Company. Several recovery standards were added prior to the first step in the extraction process for QC purposes. To remove protein, dissociate small molecules bound to protein or trapped in the precipitated protein matrix, and to recover chemically diverse metabolites, proteins were precipitated with methanol under vigorous shaking for 2 min (Glen Mills GenoGrinder 2000) followed by centrifugation. The resulting extract was divided into five fractions: two for analysis by two separate reverse phase (RP)/UPLC-MS/MS methods with positive ion mode electrospray ionization (ESI), one for analysis by RP/UPLC-MS/MS with negative ion mode ESI, one for analysis by HILIC/UPLC-MS/MS with negative ion mode ESI, and one sample was reserved for backup. Samples were placed briefly on a TurboVap® (Zymark) to remove the organic solvent. The sample extracts were stored overnight under nitrogen before preparation for analysis.

Analysis: Four separate methods utilized the following conditions: positive ionization chromatographically optimized for hydrophilic compounds (LC-MS/MS Pos Polar), positive ionization chromatographically optimized for hydrophobic compounds (LC-MS/MS Pos Lipid), negative ionization optimized conditions (LC-MS/MS Neg), and negative ionization with HILIC chromatography (LC-MS/MS Polar). All chromatography was performed using a Waters Acquity UPLC (Waters) held at 40–50°C. The injection volume was 5 µL with a 2x loop overflow.

Mass spectrometry methods utilized Thermo Scientific Q-Exactive high resolution/accurate mass spectrometers with heated electrospray ionization (HESI-II) sources and Orbitrap mass analyzers (ThermoFisher Scientific) operated at 35 000 mass resolution. The methods alternated between full scan MS and data-dependent MS_n scans. The scan range varied between methods but generally covered 70–1000 m/z.

Compound detection: Metabolites were identified by matching the ion chromatographic retention index, accurate mass, and mass spectral fragmentation signatures with a reference library consisting of 3077 entries created from authentic standard metabolites analyzed under identical instrumental procedures as the experimental samples. Proprietary peak detection and integration software^{126, 127} was used to generate a list of m/z ratios, fragmentation spectra, retention indices, and area under the curve (AUC) values. User-specified criteria for peak detection included thresholds for signal-to-noise ratio, area, and width (further details on software methods, including peak integration, alignment, and QC protocols are available in the open-source reference¹²⁷).

Statistical analyses: Any missing values are assumed to be below the limits of detection; these values were imputed with the compound minimum (minimum value imputation). Statistical tests were performed in ArrayStudio (Omicsoft) or “R” to compare data between experimental groups; $p < 0.05$ is considered significant and $0.05 < p < 0.10$ to be trending. An estimate of the false discovery rate (Q-value) was also calculated to take into account the multiple comparisons that normally occur in metabolomic-based studies, with $q < 0.05$ used as an indication of high confidence in a result. To identify candidate metabolites potentially mediating the effect of serum on aNPC proliferation, we adopted a biologically informed strategy rather than a conventional untargeted differential analysis. Specifically, we first screened for metabolites whose levels significantly correlated ($p < 0.01$) with the BBA-derived proliferation index and anxiety scores. This correlation-driven selection yielded three top candidates: LPA16:0, fibrinopeptide B, and LPS 18:0. We then evaluated their differential abundance across groups (HR susceptible, HR resilient, controls) using one-way ANOVA. As this approach was hypothesis-driven and involved a limited number of follow-up comparisons, false discovery rate (FDR) correction was not applied, given its primary relevance in high-dimensional exploratory settings. The total number of metabolites assessed in the untargeted metabolomics dataset was 1049, which served exclusively for the initial correlation screen (Supplementary data).

Targeted LPA quantification:

Mouse sera (15 μ L) were extracted with 75 μ L of ice-cold isopropanol (IPA) spiked with C17 cLPA as the internal standard (IS). To promote the lipid extraction and protein precipitation this solution was vortexed and centrifuged (at 4°C for 15 minutes at 14000rpm). The resulting supernatant was analyzed by reversed phase Liquid chromatography coupled to tandem mass spectrometry (RPLC-MS/MS) in negative ionization mode operating in selective reaction monitoring mode (SRM, TSQ Altis triple quadrupole system interfaced with a Vanquish UHPLC system (Thermo Fisher Scientific)). Chromatographic separation was carried out on a Zorbax Eclipse Plus C18 (1.8 μ m, 100 mm \times 2.1 mm I.D.) column (Agilent technologies, USA). Mobile phase was composed of A = 60:40 (v/v Acetonitrile: water solution) with 10 mM ammonium acetate and 0.1% acetic acid and B = 88:10:2 (Isopropanol: acetonitrile: water solution) with 10 mM ammonium acetate and 0.1% acetic acid. The linear gradient elution from 15% to 30% B was applied for 2 minutes, then from 30% to 48% B for 0.5 minutes, from 48% to 72% B and last gradient step from 72% to 99% B followed by 0.5 minutes isocratic conditions and a 3 min re-equilibration to the initial chromatographic conditions. The flow rate was 600 μ L/min, column temperature 60 °C and

sample injection volume 2µl. Data were processed using XCalibur 4.3 (Thermo Fisher Scientific) and concentrations were calculated to IS using a calibration curve.

Genetic analyses of the PsyMetab cohort

All participants were genotyped on the Global Screening Array (GSA) v2 with multiple disease option (MD) chip at iGE3 institute in Geneva, Switzerland (<http://www.ige3.unige.ch/genomics-platform.php>). All quality control (QC) and filtering steps were performed in PLINK¹²⁸. Ancestry was determined using Snpweights, a software for inferring genome-wide (GW) ancestry using SNP weights precomputed from large external reference panels¹²⁹. Only individuals from European ancestry were considered in the present study. Multivariable logistic mixed models adjusting for age, sex, smoking and body mass index were conducted to test associations between SNPs and the anxiety phenotype. A dominant transmission was considered for rs10817103C>T (i.e., patients carrying the T allele were compared to patients carrying the CC genotype). Statistical significance was defined as a p value ≤ 0.05 . Statistical analyses were performed using Stata 14 (StataCorp, College Station TX, USA) and R environment for statistical computing version 4.1.1.

Single-cell RNA sequencing

Mouse Dataset

Pre-processed unique molecular identifiers (UMI) count matrix from a published single-cell RNA-sequencing dataset⁵⁸ was retrieved from the respective repository [GEO: GSE104323] and processed using the R package Seurat (v4.4.0)¹³⁰. To focus the analysis on adult brain, only data from older-age timepoints (P120 and P132) were subsetted and retained for downstream analysis. The pre-processed UMI count matrices were normalized using the NormalizeData() function in Seurat with a scaling factor of 10,000. To enable visualization of cells with similar transcriptomic profiles in two-dimensional space, the top 2,000 highly variable genes were identified using the FindVariableFeatures() function with the default variance stabilizing transformation. Dimensionality reduction was then performed using RunPCA() and RunUMAP(). Clustering analysis was carried out using the FindNeighbors() and FindClusters() functions. Cell type annotations were retrieved from the accompanying metadata of the original dataset and used for visualization in two-dimensional space.

Human Datasets

We analyzed a publicly available single-cell RNA-sequencing dataset from human brain tissue⁶⁰, accessed via [<https://zenodo.org/records/14879680>]. Data processing was carried out in R using Seurat (v4.4.0)¹³⁰. To restrict the analysis to adult samples, only individuals aged 20 years and older were included. UMI count matrices were normalized using `NormalizeData()` with a scaling factor of 10,000. Gene selection was performed using `FindVariableFeatures()` to identify the top 2,000 highly variable genes. Dimensionality reduction was conducted via `RunPCA()` and `RunUMAP()` to visualize transcriptomic similarities across cells. To correct for donor-specific expression differences, we applied Harmony integration (v1.1.0) with the following parameters: `kmeans_init_nstart = 20`, `kmeans_init_iter_max = 150`, using 'sample' as the batch indicator. Cell clusters were identified using `FindNeighbors()` and `FindClusters()`. Cell type annotations provided in the original metadata were retained and used for visualization.

Samples were processed as described in Tosoni et al.⁶¹. From a total of 110,527 high quality nuclei, control samples (n=24,655) were subsetted for exploring LPAR1 gene expression in all cell types and subsequently in a subset including all granular cell types (n=13,446). Raw UMI counts were normalized using the 'NormalizeData' function, with the scaling factor equal to 10,000. Top 2000 variable features were selected with the function `FindVariableFeatures`, and data were scaled using the `ScaleData` function. The dimensionality of the data was first reduced by principal component analysis (PCA). To account for large differences in expression across donors, as well as for technical batch effects, principal components were aligned with Harmony (v1.1.0 with `kmeans_init_nstart=20`, `kmeans_init_iter_max=150`, `lambda=1` options) using 'sample' and 'run' as batch indicators. The corrected components (dims=1:20) were then used for constructing a neighborhood graph and for clustering the nuclei based on transcription similarity using the Louvain algorithm (`FindNeighbors` `FindClusters`) and applying appropriate 1.4 resolution. Finally, clusters were visualized with uniform manifold approximation and projection (UMAP). All of the above functions are part of the Seurat R Package 4.4.0.

Statistical analysis

All statistical tests except for single-cell RNA sequencing, were performed with GraphPad Prism (San Diego, CA, USA) using a critical probability of $p < 0.05$. Statistical analyses performed for each experiment are summarized in each figure legend with the chosen statistical test, sample size 'n' and p values, as well as degree of freedom and F/t values. All values are given as mean \pm S.E.M.

Data availability

The data presented in this study is provided in the Source Data file and is publicly available on Zenodo: <https://doi.org/10.5281/zenodo.18076116>. The metabolomics data is publicly available on Metaboliqts: <https://www.ebi.ac.uk/metaboliqts/MTBLS13589>.

Source data are provided with this paper.

References:

1. Penninx BW, Pine DS, Holmes EA, Reif A. Anxiety disorders. *Lancet* **397**, 914-927 (2021).
2. Gustavsson A, *et al.* Cost of disorders of the brain in Europe 2010. *Eur Neuropsychopharmacol* **21**, 718-779 (2011).
3. Braga RJ, Reynolds GP, Siris SG. Anxiety comorbidity in schizophrenia. *Psychiatry Res* **210**, 1-7 (2013).
4. Goldstein-Piekarski AN, Williams LM, Humphreys K. A trans-diagnostic review of anxiety disorder comorbidity and the impact of multiple exclusion criteria on studying clinical outcomes in anxiety disorders. *Transl Psychiatry* **6**, e847 (2016).
5. Lamers F, *et al.* Comorbidity patterns of anxiety and depressive disorders in a large cohort study: the Netherlands Study of Depression and Anxiety (NESDA). *J Clin Psychiatry* **72**, 341-348 (2011).
6. Pavlova B, *et al.* Prevalence of current anxiety disorders in people with bipolar disorder during euthymia: a meta-analysis. *Psychol Med* **47**, 1107-1115 (2017).
7. Romanazzo S, Mansueto G, Cosci F. Anxiety in the Medically Ill: A Systematic Review of the Literature. *Front Psychiatry* **13**, 873126 (2022).
8. Shepardson RL, Buchholz LJ, Weisberg RB, Funderburk JS. Psychological interventions for anxiety in adult primary care patients: A review and recommendations for future research. *J Anxiety Disord* **54**, 71-86 (2018).
9. Weisberg RB, Beard C, Moitra E, Dyck I, Keller MB. Adequacy of treatment received by primary care patients with anxiety disorders. *Depress Anxiety* **31**, 443-450 (2014).
10. Sandi C, Richter-Levin G. From high anxiety trait to depression: a neurocognitive hypothesis. *Trends Neurosci* **32**, 312-320 (2009).
11. Lehmann ML, Brachman RA, Martinowich K, Schloesser RJ, Herkenham M. Glucocorticoids orchestrate divergent effects on mood through adult neurogenesis. *J Neurosci* **33**, 2961-2972 (2013).
12. McEwen BS, *et al.* Mechanisms of stress in the brain. *Nat Neurosci* **18**, 1353-1363 (2015).

13. Surget A, Belzung C. Adult hippocampal neurogenesis shapes adaptation and improves stress response: a mechanistic and integrative perspective. *Mol Psychiatry* **27**, 403-421 (2022).
14. Altman J, Das GD. Post-natal origin of microneurons in the rat brain. *Nature* **207**, 953-956 (1965).
15. Stranahan AM, Khalil D, Gould E. Social isolation delays the positive effects of running on adult neurogenesis. *Nat Neurosci* **9**, 526-533 (2006).
16. Goshen I, *et al.* Brain interleukin-1 mediates chronic stress-induced depression in mice via adrenocortical activation and hippocampal neurogenesis suppression. *Mol Psychiatry* **13**, 717-728 (2008).
17. Lucassen PJ, *et al.* Regulation of Adult Neurogenesis and Plasticity by (Early) Stress, Glucocorticoids, and Inflammation. *Cold Spring Harb Perspect Biol* **7**, a021303 (2015).
18. Anacker C, Hen R. Adult hippocampal neurogenesis and cognitive flexibility - linking memory and mood. *Nat Rev Neurosci* **18**, 335-346 (2017).
19. Czeh B, *et al.* Chronic psychosocial stress and concomitant repetitive transcranial magnetic stimulation: effects on stress hormone levels and adult hippocampal neurogenesis. *Biol Psychiatry* **52**, 1057-1065 (2002).
20. Gould E, McEwen BS, Tanapat P, Galea LA, Fuchs E. Neurogenesis in the dentate gyrus of the adult tree shrew is regulated by psychosocial stress and NMDA receptor activation. *J Neurosci* **17**, 2492-2498 (1997).
21. Mirescu C, Peters JD, Gould E. Early life experience alters response of adult neurogenesis to stress. *Nat Neurosci* **7**, 841-846 (2004).
22. Egeland M, Zunszain PA, Pariante CM. Molecular mechanisms in the regulation of adult neurogenesis during stress. *Nat Rev Neurosci* **16**, 189-200 (2015).
23. Toda T, Parylak SL, Linker SB, Gage FH. The role of adult hippocampal neurogenesis in brain health and disease. *Mol Psychiatry* **24**, 67-87 (2019).
24. Anacker C, *et al.* Hippocampal neurogenesis confers stress resilience by inhibiting the ventral dentate gyrus. *Nature* **559**, 98-102 (2018).
25. Snyder JS, Soumier A, Brewer M, Pickel J, Cameron HA. Adult hippocampal neurogenesis buffers stress responses and depressive behaviour. *Nature* **476**, 458-461 (2011).
26. Surget A, *et al.* Antidepressants recruit new neurons to improve stress response regulation. *Mol Psychiatry* **16**, 1177-1188 (2011).
27. Santarelli L, *et al.* Requirement of hippocampal neurogenesis for the behavioral effects of antidepressants. *Science* **301**, 805-809 (2003).
28. Hill AS, Sahay A, Hen R. Increasing Adult Hippocampal Neurogenesis is Sufficient to Reduce Anxiety and Depression-Like Behaviors. *Neuropsychopharmacology* **40**, 2368-2378 (2015).
29. Palmer TD, Willhoite AR, Gage FH. Vascular niche for adult hippocampal neurogenesis. *J Comp Neurol* **425**, 479-494 (2000).
30. Sun GJ, *et al.* Tangential migration of neuronal precursors of glutamatergic neurons in the adult mammalian brain. *Proc Natl Acad Sci U S A* **112**, 9484-9489 (2015).

31. Licht T, *et al.* Hippocampal neural stem cells facilitate access from circulation via apical cytoplasmic processes. *Elife* **9**, (2020).
32. Moss J, *et al.* Fine processes of Nestin-GFP-positive radial glia-like stem cells in the adult dentate gyrus ensheath local synapses and vasculature. *Proc Natl Acad Sci U S A* **113**, E2536-2545 (2016).
33. De Miguel Z, *et al.* Exercise plasma boosts memory and dampens brain inflammation via clusterin. *Nature* **600**, 494-499 (2021).
34. Horowitz AM, *et al.* Blood factors transfer beneficial effects of exercise on neurogenesis and cognition to the aged brain. *Science* **369**, 167-173 (2020).
35. Katsimpardi L, *et al.* Vascular and neurogenic rejuvenation of the aging mouse brain by young systemic factors. *Science* **344**, 630-634 (2014).
36. Smith LK, *et al.* beta2-microglobulin is a systemic pro-aging factor that impairs cognitive function and neurogenesis. *Nat Med* **21**, 932-937 (2015).
37. Villeda SA, *et al.* The ageing systemic milieu negatively regulates neurogenesis and cognitive function. *Nature* **477**, 90-94 (2011).
38. Villeda SA, *et al.* Young blood reverses age-related impairments in cognitive function and synaptic plasticity in mice. *Nat Med* **20**, 659-663 (2014).
39. Hollis F, van der Kooij MA, Zanoletti O, Lozano L, Canto C, Sandi C. Mitochondrial function in the brain links anxiety with social subordination. *Proc Natl Acad Sci U S A* **112**, 15486-15491 (2015).
40. Nasca C, Bigio B, Zelli D, Nicoletti F, McEwen BS. Mind the gap: glucocorticoids modulate hippocampal glutamate tone underlying individual differences in stress susceptibility. *Mol Psychiatry* **20**, 755-763 (2015).
41. Anacker C, *et al.* Glucocorticoid-related molecular signaling pathways regulating hippocampal neurogenesis. *Neuropsychopharmacology* **38**, 872-883 (2013).
42. Jung S, *et al.* Autophagic death of neural stem cells mediates chronic stress-induced decline of adult hippocampal neurogenesis and cognitive deficits. *Autophagy* **16**, 512-530 (2020).
43. Belzung C, Griebel G. Measuring normal and pathological anxiety-like behaviour in mice: a review. *Behav Brain Res* **125**, 141-149 (2001).
44. Lau T, Bigio B, Zelli D, McEwen BS, Nasca C. Stress-induced structural plasticity of medial amygdala stellate neurons and rapid prevention by a candidate antidepressant. *Mol Psychiatry* **22**, 227-234 (2017).
45. Nasca C, *et al.* Stress dynamically regulates behavior and glutamatergic gene expression in hippocampus by opening a window of epigenetic plasticity. *Proc Natl Acad Sci U S A* **112**, 14960-14965 (2015).
46. Birmaher B, *et al.* Lifetime psychiatric disorders in school-aged offspring of parents with bipolar disorder: the Pittsburgh Bipolar Offspring study. *Arch Gen Psychiatry* **66**, 287-296 (2009).
47. Dean K, Stevens H, Mortensen PB, Murray RM, Walsh E, Pedersen CB. Full spectrum of psychiatric outcomes among offspring with parental history of mental disorder. *Arch Gen Psychiatry* **67**, 822-829 (2010).

48. Franke B, *et al.* The genetics of attention deficit/hyperactivity disorder in adults, a review. *Mol Psychiatry* **17**, 960-987 (2012).
49. Lau P, Hawes DJ, Hunt C, Frankland A, Roberts G, Mitchell PB. Prevalence of psychopathology in bipolar high-risk offspring and siblings: a meta-analysis. *Eur Child Adolesc Psychiatry* **27**, 823-837 (2018).
50. Mesman E, Nolen WA, Reichart CG, Wals M, Hillegers MH. The Dutch bipolar offspring study: 12-year follow-up. *Am J Psychiatry* **170**, 542-549 (2013).
51. Vandeleur C, *et al.* Mental disorders in offspring of parents with bipolar and major depressive disorders. *Bipolar Disord* **14**, 641-653 (2012).
52. Smith AK, Mick E, Faraone SV. Advances in genetic studies of attention-deficit/hyperactivity disorder. *Curr Psychiatry Rep* **11**, 143-148 (2009).
53. Geraldo LHM, *et al.* Role of lysophosphatidic acid and its receptors in health and disease: novel therapeutic strategies. *Signal Transduct Target Ther* **6**, 45 (2021).
54. Yung YC, Stoddard NC, Mirendil H, Chun J. Lysophosphatidic Acid signaling in the nervous system. *Neuron* **85**, 669-682 (2015).
55. Stefan C, Jansen S, Bollen M. NPP-type ectophosphodiesterases: unity in diversity. *Trends Biochem Sci* **30**, 542-550 (2005).
56. Suckau O, *et al.* LPA(1) , LPA(2) , LPA(4) , and LPA(6) receptor expression during mouse brain development. *Dev Dyn* **248**, 375-395 (2019).
57. Walker TL, *et al.* Lysophosphatidic Acid Receptor Is a Functional Marker of Adult Hippocampal Precursor Cells. *Stem Cell Reports* **6**, 552-565 (2016).
58. Hochgerner H, Zeisel A, Lonnerberg P, Linnarsson S. Conserved properties of dentate gyrus neurogenesis across postnatal development revealed by single-cell RNA sequencing. *Nat Neurosci* **21**, 290-299 (2018).
59. Redmond SA, *et al.* Development of Ependymal and Postnatal Neural Stem Cells and Their Origin from a Common Embryonic Progenitor. *Cell Rep* **27**, 429-441 e423 (2019).
60. Dumitru I, *et al.* Identification of proliferating neural progenitors in the adult human hippocampus. *Science* **389**, 58-63 (2025).
61. Tosoni G, *et al.* Unique transcriptional profiles of adult human immature neurons in healthy aging, Alzheimer's disease, and cognitive resilience. *bioRxiv*, 2025.2001.2008.631686 (2025).
62. Canela-Xandri O, Rawlik K, Tenesa A. An atlas of genetic associations in UK Biobank. *Nat Genet* **50**, 1593-1599 (2018).
63. Consortium GT. The Genotype-Tissue Expression (GTEx) project. *Nat Genet* **45**, 580-585 (2013).
64. Golden SA, *et al.* Epigenetic regulation of RAC1 induces synaptic remodeling in stress disorders and depression. *Nat Med* **19**, 337-344 (2013).
65. Zimprich A, *et al.* A robust and reliable non-invasive test for stress responsivity in mice. *Front Behav Neurosci* **8**, 125 (2014).

66. Bottes S, *et al.* Long-term self-renewing stem cells in the adult mouse hippocampus identified by intravital imaging. *Nat Neurosci* **24**, 225-233 (2021).
67. Rivera RR, Lin ME, Bornhop EC, Chun J. Conditional Lpar1 gene targeting identifies cell types mediating neuropathic pain. *FASEB J* **34**, 8833-8842 (2020).
68. Eichholtz T, Jalink K, Fahrenfort I, Moolenaar WH. The bioactive phospholipid lysophosphatidic acid is released from activated platelets. *Biochem J* **291 (Pt 3)**, 677-680 (1993).
69. Ghatge M, Flora GD, Nayak MK, Chauhan AK. Platelet Metabolic Profiling Reveals Glycolytic and 1-Carbon Metabolites Are Essential for GP VI-Stimulated Human Platelets-Brief Report. *Arterioscler Thromb Vasc Biol* **44**, 409-416 (2024).
70. Aoki J. Mechanisms of lysophosphatidic acid production. *Semin Cell Dev Biol* **15**, 477-489 (2004).
71. Aoki J, *et al.* Serum lysophosphatidic acid is produced through diverse phospholipase pathways. *J Biol Chem* **277**, 48737-48744 (2002).
72. Boucharaba A, *et al.* Platelet-derived lysophosphatidic acid supports the progression of osteolytic bone metastases in breast cancer. *J Clin Invest* **114**, 1714-1725 (2004).
73. Langer HF, *et al.* Platelets contribute to the pathogenesis of experimental autoimmune encephalomyelitis. *Circ Res* **110**, 1202-1210 (2012).
74. Leiter O, *et al.* Exercise-Induced Activated Platelets Increase Adult Hippocampal Precursor Proliferation and Promote Neuronal Differentiation. *Stem Cell Reports* **12**, 667-679 (2019).
75. Shin J, *et al.* Single-Cell RNA-Seq with Waterfall Reveals Molecular Cascades underlying Adult Neurogenesis. *Cell Stem Cell* **17**, 360-372 (2015).
76. Boldrini M, *et al.* Human Hippocampal Neurogenesis Persists throughout Aging. *Cell Stem Cell* **22**, 589-599 e585 (2018).
77. Boldrini M, *et al.* Resilience Is Associated With Larger Dentate Gyrus, While Suicide Decedents With Major Depressive Disorder Have Fewer Granule Neurons. *Biol Psychiatry* **85**, 850-862 (2019).
78. Kempermann G, *et al.* Human Adult Neurogenesis: Evidence and Remaining Questions. *Cell Stem Cell* **23**, 25-30 (2018).
79. Moreno-Jimenez EP, *et al.* Adult hippocampal neurogenesis is abundant in neurologically healthy subjects and drops sharply in patients with Alzheimer's disease. *Nat Med* **25**, 554-560 (2019).
80. Sorrells SF, *et al.* Human hippocampal neurogenesis drops sharply in children to undetectable levels in adults. *Nature* **555**, 377-381 (2018).
81. Terreros-Roncal J, *et al.* Impact of neurodegenerative diseases on human adult hippocampal neurogenesis. *Science* **374**, 1106-1113 (2021).
82. Du Preez A, *et al.* The serum metabolome mediates the concert of diet, exercise, and neurogenesis, determining the risk for cognitive decline and dementia. *Alzheimers Dement* **18**, 654-675 (2022).
83. Maruszak A, *et al.* Predicting progression to Alzheimer's disease with human hippocampal progenitors exposed to serum. *Brain* **146**, 2045-2058 (2023).

84. Borsini A, *et al.* The role of circulatory systemic environment in predicting interferon-alpha-induced depression: The neurogenic process as a potential mechanism. *Brain Behav Immun* **81**, 220-227 (2019).
85. Toews ML, Ustinova EE, Schultz HD. Lysophosphatidic acid enhances contractility of isolated airway smooth muscle. *J Appl Physiol (1985)* **83**, 1216-1222 (1997).
86. Gerrard JM, Kindom SE, Peterson DA, Peller J, Krantz KE, White JG. Lysophosphatidic acids. Influence on platelet aggregation and intracellular calcium flux. *Am J Pathol* **96**, 423-438 (1979).
87. Lee D, Kim YH, Kim JH. The Role of Lysophosphatidic Acid in Adult Stem Cells. *Int J Stem Cells* **13**, 182-191 (2020).
88. Benesch MG, *et al.* Autotaxin is an inflammatory mediator and therapeutic target in thyroid cancer. *Endocr Relat Cancer* **22**, 593-607 (2015).
89. Moreno-Fernandez RD, *et al.* maLPA1-null mice as an endophenotype of anxious depression. *Transl Psychiatry* **7**, e1077 (2017).
90. Rosell-Valle C, *et al.* Chronic central modulation of LPA/LPA receptors-signaling pathway in the mouse brain regulates cognition, emotion, and hippocampal neurogenesis. *Prog Neuropsychopharmacol Biol Psychiatry* **108**, 110156 (2021).
91. Moreno-Fernandez RD, *et al.* Stress, Depression, Resilience and Ageing: A Role for the LPA-LPA1 Pathway. *Curr Neuropharmacol* **16**, 271-283 (2018).
92. Burnouf T, Walker TL. The multifaceted role of platelets in mediating brain function. *Blood* **140**, 815-827 (2022).
93. Leiter O, Walker TL. Platelets: The missing link between the blood and brain? *Prog Neurobiol* **183**, 101695 (2019).
94. Hayon Y, Dashevsky O, Shai E, Brill A, Varon D, Leker RR. Platelet microparticles induce angiogenesis and neurogenesis after cerebral ischemia. *Curr Neurovasc Res* **9**, 185-192 (2012).
95. Kazanis I, *et al.* Lesion-induced accumulation of platelets promotes survival of adult neural stem / progenitor cells. *Exp Neurol* **269**, 75-89 (2015).
96. Hayon Y, Dashevsky O, Shai E, Varon D, Leker RR. Platelet lysates stimulate angiogenesis, neurogenesis and neuroprotection after stroke. *Thromb Haemost* **110**, 323-330 (2013).
97. Kaneez FS, Saeed SA. Investigating GABA and its function in platelets as compared to neurons. *Platelets* **20**, 328-333 (2009).
98. Begni B, *et al.* Substrate-induced modulation of glutamate uptake in human platelets. *Br J Pharmacol* **145**, 792-799 (2005).
99. Yamamoto H, Gurney ME. Human platelets contain brain-derived neurotrophic factor. *J Neurosci* **10**, 3469-3478 (1990).
100. Musselman DL, *et al.* Exaggerated platelet reactivity in major depression. *Am J Psychiatry* **153**, 1313-1317 (1996).
101. Chen Z, Wang J, Carru C, Sedda S, Nivoli AM, Li Z. Meta-analysis of peripheral mean platelet volume in patients with mental disorders: Comparisons in depression, anxiety, bipolar disorder, and schizophrenia. *Brain Behav* **13**, e3240 (2023).

102. Leiter O, *et al.* Platelet-derived exerkine CXCL4/platelet factor 4 rejuvenates hippocampal neurogenesis and restores cognitive function in aged mice. *Nat Commun* **14**, 4375 (2023).
103. Min Y, *et al.* Platelets fine-tune effector responses of naive CD4(+) T cells via platelet factor 4-regulated transforming growth factor beta signaling. *Cell Mol Life Sci* **79**, 247 (2022).
104. Benesch MG, Zhao YY, Curtis JM, McMullen TP, Brindley DN. Regulation of autotaxin expression and secretion by lysophosphatidate and sphingosine 1-phosphate. *J Lipid Res* **56**, 1134-1144 (2015).
105. Kappelmann N, *et al.* Dissecting the Association Between Inflammation, Metabolic Dysregulation, and Specific Depressive Symptoms: A Genetic Correlation and 2-Sample Mendelian Randomization Study. *JAMA Psychiatry* **78**, 161-170 (2021).
106. Michopoulos V, Powers A, Gillespie CF, Ressler KJ, Jovanovic T. Inflammation in Fear- and Anxiety-Based Disorders: PTSD, GAD, and Beyond. *Neuropsychopharmacology* **42**, 254-270 (2017).
107. Milaneschi Y, *et al.* Association of inflammation with depression and anxiety: evidence for symptom-specificity and potential causality from UK Biobank and NESDA cohorts. *Mol Psychiatry* **26**, 7393-7402 (2021).
108. Saccaro LF, Schilliger Z, Perroud N, Pigué C. Inflammation, Anxiety, and Stress in Attention-Deficit/Hyperactivity Disorder. *Biomedicines* **9**, (2021).
109. Palmer TD, Takahashi J, Gage FH. The adult rat hippocampus contains primordial neural stem cells. *Mol Cell Neurosci* **8**, 389-404 (1997).
110. Carrard A, *et al.* Role of adult hippocampal neurogenesis in the antidepressant actions of lactate. *Mol Psychiatry* **26**, 6723-6735 (2021).
111. Cherix A, *et al.* Metabolic signature in nucleus accumbens for anti-depressant-like effects of acetyl-L-carnitine. *Elife* **9**, (2020).
112. Larrieu T, *et al.* Hierarchical Status Predicts Behavioral Vulnerability and Nucleus Accumbens Metabolic Profile Following Chronic Social Defeat Stress. *Curr Biol* **27**, 2202-2210 e2204 (2017).
113. Kedia S, Chattarji S. Marble burying as a test of the delayed anxiogenic effects of acute immobilisation stress in mice. *J Neurosci Methods* **233**, 150-154 (2014).
114. Deng W, Gage FH. The effect of immature adult-born dentate granule cells on hyponeophagial behavior is related to their roles in learning and memory. *Front Syst Neurosci* **9**, 34 (2015).
115. Heinz DE, *et al.* Exploratory drive, fear, and anxiety are dissociable and independent components in foraging mice. *Transl Psychiatry* **11**, 318 (2021).
116. Harrison DJ, *et al.* Unified Behavioral Scoring for Preclinical Models. *Front Neurosci* **14**, 313 (2020).
117. Bosch-Bouju C, Larrieu T, Linders L, Manzoni OJ, Laye S. Endocannabinoid-Mediated Plasticity in Nucleus Accumbens Controls Vulnerability to Anxiety after Social Defeat Stress. *Cell Rep* **16**, 1237-1242 (2016).
118. Di Miceli M, *et al.* Dietary Long-Chain n-3 Polyunsaturated Fatty Acid Supplementation Alters Electrophysiological Properties in the Nucleus Accumbens and Emotional Behavior in Naive and Chronically Stressed Mice. *Int J Mol Sci* **23**, (2022).

119. Sultan S, Gebara EG, Moullec K, Toni N. D-serine increases adult hippocampal neurogenesis. *Front Neurosci* **7**, 155 (2013).
120. Endler NS, Cox BJ, Parker JD, Bagby RM. Self-reports of depression and state-trait anxiety: evidence for differential assessment. *J Pers Soc Psychol* **63**, 832-838 (1992).
121. Choong E, *et al.* Influence of CRT1 polymorphisms on body mass index and fat mass in psychiatric patients and the general adult population. *JAMA Psychiatry* **70**, 1011-1019 (2013).
122. Choong E, Solida A, Lechaire C, Conus P, Eap CB. [Follow-up of the metabolic syndrome induced by atypical antipsychotics: recommendations and pharmacogenetics perspectives]. *Rev Med Suisse* **4**, 1994-1996, 1998-1999 (2008).
123. Vannoy CH, Leroy V, Broniowska K, Lu QL. Metabolomics Analysis of Skeletal Muscles from FKRP-Deficient Mice Indicates Improvement After Gene Replacement Therapy. *Sci Rep* **9**, 10070 (2019).
124. Yanckello LM, *et al.* Caloric Restriction Alters Postprandial Responses of Essential Brain Metabolites in Young Adult Mice. *Front Nutr* **6**, 90 (2019).
125. Ford L, *et al.* Precision of a Clinical Metabolomics Profiling Platform for Use in the Identification of Inborn Errors of Metabolism. *J Appl Lab Med* **5**, 342-356 (2020).
126. DeHaven CD, Evans AM, Dai H, Lawton KA. Organization of GC/MS and LC/MS metabolomics data into chemical libraries. *J Cheminform* **2**, 9 (2010).
127. DeHaven CD EA, Dai H, Lawton KA. Software techniques for enabling high-throughput analysis of metabolomics datasets. *InTech Open*, (2012).
128. Chang CC, Chow CC, Tellier LC, Vattikuti S, Purcell SM, Lee JJ. Second-generation PLINK: rising to the challenge of larger and richer datasets. *Gigascience* **4**, 7 (2015).
129. Chen CY, Pollack S, Hunter DJ, Hirschhorn JN, Kraft P, Price AL. Improved ancestry inference using weights from external reference panels. *Bioinformatics* **29**, 1399-1406 (2013).
130. Butler A, Hoffman P, Smibert P, Papalexi E, Satija R. Integrating single-cell transcriptomic data across different conditions, technologies, and species. *Nat Biotechnol* **36**, 411-420 (2018).

Acknowledgments:

The authors wish to thank Rebecca Borreggine and Tony Teav for technical assistance with mass spectrometry analyses, Fulvio Magara and Benjamin Boury-Jamot for help with animal behavioral experiments and the Cellular Imaging Facility of the University of Lausanne, for their assistance with microscopy. This work was supported by the Swiss National Science Foundation (Nb. 823 32003B_156914 to CP, 31003A_173128 and 310030_201015 to NT) and by the Swiss National

Center of Competence in Research; “Synapsy: the Synaptic Basis of Mental Diseases” (Nb. 51NF40-185897 to CP). LT was supported by an ERC starting grant (CERDEV_759112).

Author contributions:

Conceptualization: NT, TL

Methodology: TL, CC, FG, MV, CW, KG, AD, HGA, MT, HAC, JI, LT

Investigation: TL, CC, FG, MV, ES, GT, DA, AD, HAC, MT

Funding acquisition: NT, CP, AD, PM, CBE

Supervision: NT, CBE, HAC, JL, CP

Writing: TL, NT, AD, CBE, ES, JI, LT, CP, HAC, CBE, PM, CP

Competing interest statement:

Nicolas Toni and Thomas Larrieu have filed a patent application.

Patent applicant: Centre Hospitalier Universitaire Vaudois (CHUV), Lausanne, Switzerland (institutional applicant). Inventors: Nicolas Toni and Thomas Larrieu. Application number: PCT/EP2025/064764. Status of application: International patent application pending (PCT). Specific aspect of the manuscript covered by the patent application: Therapeutic methods targeting LPA16:0–LPAR1/LPAR3 signaling for the treatment and/or prevention of neuropsychiatric and emotional dysregulation disorders, particularly anxiety-related phenotypes. Diagnostic methods and kits for measuring circulating LPA16:0 levels in biological samples to stratify subjects (e.g. high- vs low-anxiety, stress susceptibility/resilience). Use of LPA16:0 as a biomarker linked to hippocampal neurogenesis and stress resilience, including pharmacological modulation of LPAR1/3 activity.

Reporting summary

Further information on research design is available in the Nature Portfolio Reporting Summary linked to this article.

Figure legends

Fig. 1: Serum from anxious mice reduces aNPC proliferation *in vitro*.

a. Schematic illustration of the BBA assay. **b.** Proportion of aNPC that incorporated BrdU after exposure to serum pooled from 4 adult C57BL/6J male mice at different concentrations for 24 hours under coating conditions. $F_{4,24} = 23.32$, $p = 5.7E-8$, one-way ANOVA; Tukey's multiple comparisons with the mean of CTRL group. Data points show 2 wells per condition for 3 biological replicates for a total of $n=6$, except for 2% serum (1 well missing in one biological replicate, $n=5$). **c, d.** Number (**c**) and mean size (**d**) of neurospheres after exposure to serum from 4 adult C57BL/6J mice at different concentrations for 72 hours. Neurospheres number: $F_{2,27} = 40.12$, $p = 8.2E-09$, one-way ANOVA; Tukey's multiple comparisons with the mean of CTRL group; Neurospheres size: $F_{2,27} = 13.55$, $p = 8.4E-05$, one-way ANOVA; Tukey's multiple comparisons with the mean of CTRL group. The number and mean size of neurospheres were counted in 4 selected fields per well, 3 wells per condition from 3 independent replicates. **e.** Representative bright field image of neurospheres (out of 36 images per group). **f.** Experimental design. **g.** Grouped heatmap of the time spent in the open (vertical) and closed (horizontal) arms of an EPM for low (LA) and high (HA) anxious mice. **h-i.** Violin plot (**h**) and histogram (**i**) of the anxiety score of LA and HA mice. **l.** $t_{22} = 6.79$, $p = 8E-07$, unpaired t-test, two-tailed, $n = 12$ per group. **j (left).** Histogram of aNPC proliferation in the BBA assay after exposure to serum from HA or LA mice ($t_{22} = 2.55$, $p = 0.018$, unpaired t-test, two-tailed, $n = 12$ per group). **j (right):** Representative confocal micrographs of aNPC immunostained for BrdU and DAPI after exposure to serum from LA and HA mice. **k.** Correlation plot between *in vitro* proliferation and trait anxiety score. Pearson's product-moment correlation with two-tailed tests ($p = 0.0029$). **l.** Histogram of the free serum corticosterone ($t_{22} = 0,3519$, $p > 0.05$ unpaired t-test, two-tailed, $n = 12$ per group). **m.** Correlation plot between *in vitro* cell proliferation and free corticosterone. **n.** Experimental design. **o.** Body weight change over time in CTRL ($n=7$) and CRS-treated mice ($n=10$) (Stress effect: $F(1, 15) = 16,61$; $p = 0,001$, Two-way ANOVA with repeated measure). **p.** Free serum corticosterone ($t_{14} = 3,021$, $p = 0.009$, unpaired t-test, two-tailed, $n = 8$ per group). **q.** State anxiety score ($t_{15} = 3.08$, $p = 0.0082$, unpaired t-test, two-tailed, $n = 8$ in Ctrl and 9 in CRS group). **r (left).** Cell proliferation in the BBA assay after treatment with serum from CRS or CTRL mice ($t_{15} = 3.11$, $p = 0.0067$, unpaired t-test, two-tailed, $n = 8$ and 9 per group). **r (right).** Representative confocal micrographs of aNPC treated with serum from CTRL or CRS mice and immunostained for BrdU (white) and DAPI (blue). **s.** Correlation plot between cell proliferation and state anxiety score. Pearson's product-moment correlation with two-tailed tests ($p = 2.3E-05$). **t.** Same data as in panel **r**, where

CRS-treated mice were subdivided in high proliferative (HP, blue) and low proliferative (LP, green). **u.** State anxiety score of CTRL (n=8), CRS-HP (n=4) and CRS-LP (n=5) mice. (Kruskal-Wallis test, post-hoc analysis for multiple comparisons: CTRL vs. CRS-LP, $p = 0.0047$; CTRL vs. CRS-HP, n.s.). **v.** Same data as in panel **q**, where CRS-treated mice were subdivided in resilient (CRS-res, blue) and susceptible (CRS-susc, green) mice. **w.** Cell proliferation in the BBA assay of CTRL (n=8), CRS-resilient (n=4) and CRS-susceptible (n=5) mice (Kruskal-Wallis test, post-hoc analysis for multiple comparisons: CTRL vs. CRS-Susc., $p = 0.0034$; CTRL vs. CRS-Res: n.s.). **x.** Receiver Operating Characteristic (ROC) curve for the discrimination of CRS-induced susceptibility by the BBA assay. **y.** Correlation between cell proliferation and free serum corticosterone. Pearson's product-moment correlation with two-tailed tests. For correlation plots, linear regression, r^2 and p values are indicated in the graphs when significant correlations were found. Histograms show average \pm SEM. ns: not significant; * $p < 0.05$; ** $p < 0.01$; *** $p < 0.001$. Source data are provided as a Source Data file.

Fig. 2: LPA16:0 increases with anxiety in patients and induces a LPA1-dependent reduction in aNSC proliferation. **a.** Schematic illustration of patients' assessment. **b.** Characteristics of the BipOff cohort. **c, d.** Trait (**c**) and state (**d**) anxiety levels in CTRL (n=29), HR-S (n=22) and HR-Res (n=15) individuals (**c**, $F_{2,65} = 15.16$, one-way ANOVA, CTRL vs. HR-S $p = 4.8E-05$; HR-S vs. HR-R $p = 0.002$); **d**, $F_{2,65} = 11.83$, one-way ANOVA, CTRL vs. HR-S $p = 0.0003$; HR-S vs. HR-R $p = 0.003$). **e.** Cell proliferation in the BBA assay after treatment with serum from CTRL (n=31), HR-S (n=22) and HR-R (n=15) individuals ($F_{2,65} = 4.06$, one-way ANOVA, CTRL vs. HR-S $p = 0.008$; HR-S vs. HR-R $p = 0.047$). **f.** Representative confocal micrographs of aNPC treated with serum from HR-S and HR-R individuals and immunostained against BrdU (green) and DAPI (blue). **g.** ROC curve for the discrimination of HR-S individuals by the BBA assay. **h, i.** Correlations between cell proliferation and trait (**h**) or state (**i**) anxiety. Pearson's product-moment correlation with two-tailed tests. **j.** Schematic illustration of the biosynthesis and degradation of LPA (Phospholipase D, PLD; Phospholipase A, PLA; Diacylglycerol kinase, DAG kinase; Secreted phospholipase A2, sPLA2; Autotaxin, ATX; Lipid phosphate phosphatase 1, LPP1; lecithin-cholesterol acyltransferase, LCAT). **k.** Correlation plot between cell proliferation and serum LPA16:0 abundance (relative values). Pearson's product-moment correlation with two-tailed tests. **l.** Serum abundance of LPA16:0 in CTRL (n=26) versus HR-S (n=19) and HR-R (n=14) individuals ($F_{2,56} = 3.10$, one-way ANOVA, CTRL vs. HR-S $p = 0.043$; HR-S vs. HR-R $p = 0.091$). **m, n.** Correlation between LPA16:0 abundance and trait (**m**) and state (**n**) anxiety levels in high-risk individuals. Pearson's product-moment correlation with

two-tailed tests. **o.** Serum phosphatidylcholine abundance in CTRL (n=29) versus HR-S (n=19) and HR-R (n=14) individuals ($F_{2,56} = 0.99$, one-way ANOVA, CTRL vs. HR-S $p = 0.012$; HR-s vs HR-R n.s). **p.** Serum lysophosphatidylcholine abundance in CTRL (n=27) versus HR-S (n=19) and HR-R (n=14) individuals ($F_{2,56} = 3.39$, $p = 0.04$, one-way ANOVA, CTRL vs HR-S $p = 0.012$; CTRL vs HR-R n.s). **q.** Serum diacylglycerol abundance in CTRL (n=27) versus HR-S (n=17) and HR-R (n=14) individuals ($F_{2,56} = 3.11$, $p = 0.05$, one-way ANOVA, CTRL vs HR-S $p = 0.009$; CTRL vs HR-R n.s). **r.** Indirect measure of ATX activity in serum from CTRL (n=28) versus HR-S (n=19) and HR-R (n=14) individuals ($F_{2,56} = 3.355$, one-way ANOVA, CTRL vs HR-S $p = 0.02$; CTRL vs HR-R n.s). **s.** Indirect measure of LPP1 activity in serum from CTRL (n=28) versus HR-S (n=19) and HR-R (n=14) individuals ($F_{2,56} = 0.738$, $p > 0.05$, one-way ANOVA). **t.** aNPC proliferation after treatment with serum from CTRL, HR-S and HR-S + KI6425 ($F_{2, 19} = 4.36$, one-way ANOVA CTRL vs. HR-S $p = 0.0054$, $n = 8$ per group, HR-S + KI6425 vs. HR-S; $p = 0.0352$, $n = 8$ per group). **u.** aNPC proliferation after cLPA16:0 treatment ($F_{4,25} = 10.17$, $p < 0.0001$, one-way ANOVA; $n = 3$ wells per condition for each replicate, 2 independent replicates. CTRL vs 30nM $p = 0.00026$). **v.** UMAP plot of data from Hochgerner et al.⁵⁸ representing 4,968 cells from adult mouse dentate gyrus. Unique molecular identifier (UMI) count matrix from the published dataset was retrieved from the respective repository and processed into the R package Seurat (4.4.0). Cells (dots) are labeled and colored by cluster membership labels from the original study. **w.** UMAP plot as in (v), colored by the level of expression of Lpar1. **x, y.** Dot plots depicting the expression profile of Lpar1 in the whole dataset (x) or only in populations belonging to the neurogenic trajectory (y). The size of each dot represents the cell percentage of this population positive for Lpar1. The scale of the dot color represents the average expression level of Lpar1 in this population. **z.** UMAP plot of data from Dumitru et al.⁶⁰ representing 179,510 cells from adult (age ≥ 20) human dentate gyrus. Unique molecular identifier (UMI) count matrix was processed into the R package Seurat (4.4.0). Cells (dots) are labeled and colored by cluster membership labels from the original study. **α.** UMAP plot as in (z), colored by the level of expression of LPAR1. **β, γ.** Dot plots depicting the expression profile of LPAR1 in the whole dataset (β) or only in subsets belonging to the granule cell neuronal population (γ). The size of each dot represents the cell percentage of this population positive for LPAR1. The scale of the dot color represents the average expression level of LPAR1 in this population. MOL, myelinating oligodendrocytes; RGL, radial glia-like cells; NB, neuroblasts; INP, intermediate neuronal progenitors. All indicated cell annotations were retrieved from the original study. For correlation plots, linear regression, r^2 and p values are indicated in the graphs. Histograms show average \pm SEM. * $p < 0.05$; *** $p < 0.001$; the absence of significance markers (asterisks) in the multiple comparisons indicates $p > 0.05$. Source

data are provided as a Source Data file.

Fig. 3: Bidirectional regulation of stress-susceptibility and neurogenesis through LPA16:0-LPA1 signaling in mice. **a.** Experimental design. **b.** Histogram of the anxiety score of LA (white, n=12) and HA (red, n=12) mice ($t_{21} = 7.029$, $p = 2.9E-7$, unpaired t-test, two-tailed). **c.** Histogram of the concentration of serum LPA16:0 ($t_{20} = 2.630$, $p = 0.016$, unpaired t-test, two-tailed, n = 11 per group). **d.** Correlation plot between LPA16:0 serum concentrations and anxiety score. Pearson's product-moment correlation with two-tailed tests. **e.** ROC curve for the discrimination of high anxious individuals by LPA16:0. **f.** Experimental design. **g.** Histogram of the anxiety score of LA (white) and HA (red) mice under at baseline (**left**; $t_{26} = 6,256$, $p = 1.28E-0.6$, unpaired t-test, two-tailed, n =14 per group), and after 5 weeks (**right**; $t_{26} = 3,375$, $p = 0.002$, unpaired t-test, and two-tailed, n =14 per group). **h.** Quantification of Ki-67⁺ cells in LA (n=11) and HA (n=10) mice (total DG, $t_{19} = 2,650$, $p = 0.0158$, unpaired t-test, two-tailed). **i.** Quantification of IdU⁺ cells in LA (n=14) and HA (n=13) mice (total DG, $t_{25} = 2,361$, $p = 0.0264$, unpaired t-test, two-tailed). **j.** Experimental design. **k.** Histogram of the anxiety score of mice treated with vehicle (white, n=6) and cLPA16:0 (orange, n=6) under baseline condition post treatment (**left**; $t_9 = 0,3932$, $p = 0.7$, unpaired t-test, two-tailed; vehicle: $t = 0.4814$, $p = 0.65$, One sample t test and cLPA16:0: $t=0.0034$, $p = 0.99$, One sample t test), and after 20 minutes acute restraint stress (**right**; $t_9 = 3.532$, $p = 0.005$, unpaired t-test, two-tailed; Vehicle: $t = 1.339$, $p = 0.2$, One sample t test and cLPA16:0: $t = 5.879$, $p = 0.002$, One sample t test). **l.** Quantification of Ki-67⁺ cells (total DG, $t_{20} = 2,109$, $p = 0.0478$, unpaired t-test, two-tailed, n = 11 per group). **m.** Cell proliferation after treatment with serum from vehicle- and cLPA16:0- treated mice ($t_{20}=2.336$, $p = 0.0295$, unpaired t-test, two-tailed, n = 11 per group). **n.** Correlation plot between serum cLPA16:0 concentration and aNPC proliferation in the BBA assay. Pearson's product-moment correlation with two-tailed tests. **o.** Experimental design. **p.** Histograms of the anxiety score of mice injected with vehicle (white) or Ki16425 (blue) under (**left**) baseline conditions ($t_{20} = 0.4336$, $p = 0.67$, unpaired t-test, two-sided; vehicle: $t = 1.044$, $p = 0.32$, One sample t test and Ki16425: $t = 1.736$, $p = 0.11$, One sample t test, n = 11 mice per group) and (**right**) after 6 hours of ARS ($t_{20} = 3.254$, $p = 0.0040$, unpaired t-test, two-tailed; vehicle: $t = 3.952$, $p = 0.0027$, One sample t test and Ki16425: $t = 1.288$, $p = 0.22$, One sample t test, n = 11 mice per group). **q.** Quantification of Ki-67⁺ cells in the DG ($t_{20} = 3.365$, $p = 0.0031$, unpaired t-test, two-tailed, n = 11 per group). **r.** Quantification of the proportion of voxels immunostained for DCX in the DG after 12 days of treatment ($t_{20} = 2.721$, $p = 0.013$, unpaired t-test, two-tailed, n = 11 per group). **s.** Histograms of the anxiety score of mice from a repetition of experiment (**o**) in an independent laboratory, under (**left**) baseline conditions

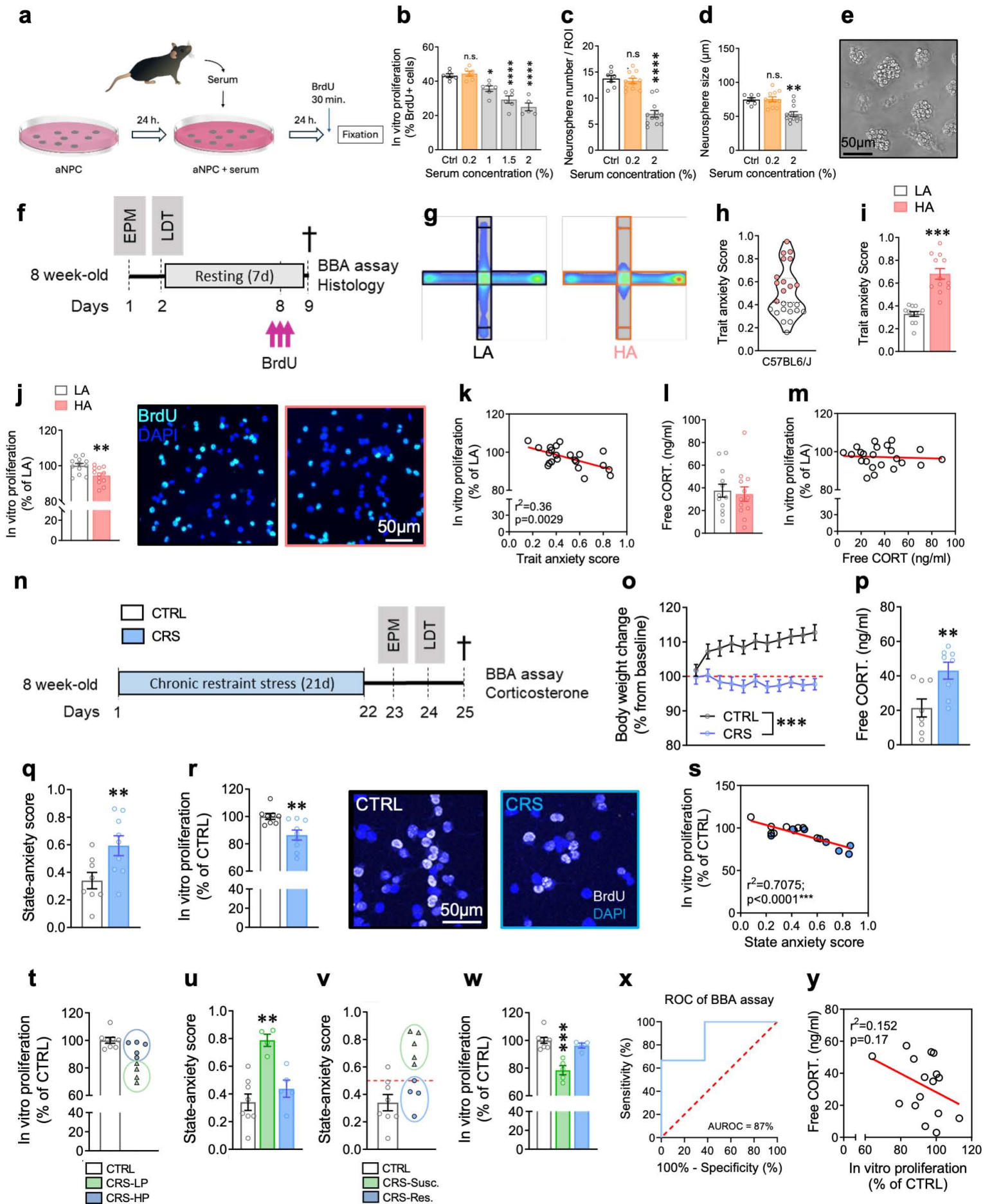
($t_{12} = 2.071$, $p = 0.06$, unpaired t-test, two-sided; vehicle: $t = 1.915$, $p = 0.1$, One sample t test and Ki16425: $t = 1.260$, $p = 0.25$, One sample t test, $n = 7$ mice per group) and **(right)** after 6 hours of ARS ($t_{12} = 2.545$, $p = 0.0257$, unpaired t-test, two-tailed; vehicle: $t = 1.993$, $p = 0.09$, One sample t test and Ki16425: $t = 1.614$, $p = 0.16$ One sample t test, $n = 7$ mice per group). **t.** Representative confocal micrographs of Ki-67 immunostaining (red) in vehicle- (left) and cLPA16:0-treated mice (right). **u.** Representative confocal micrographs of Ki-67 immunostaining (red) in vehicle- (up) and Ki16425-treated mice (down). **v.** Confocal micrographs of DCX (white) immunostaining in vehicle- (up) and Ki16425- treated mice (down). Blue: DAPI. These images are representative of 10 sections per animal for each group. **w.** Experimental design. **x.** Representative confocal micrographs of Ki-67 immunostaining (green) in Gli-LPA1^{+/+} and Gli-LPA1^{+/-} mice and quantification of Ki-67-expressing cells ($t_8 = 2.762$, $p = 0.0246$, unpaired t-test, two-tailed, $n = 5$ per group). **y.** Experimental design. **z.** Histograms of the anxiety score of mice injected with Ki16425 + NaCl (blue) and Ki16425 + TMZ (green) under **(left)** baseline conditions ($t_{12} = 1.207$, $p = 0.85$, unpaired t-test, two-sided; Ki16425 + NaCl: $t = 0.637$, $p = 0.55$, One sample t test and Ki16425 + TMZ: $t = 1.089$, $p = 0.319$, One sample t test, $n = 7$ mice per group) and **(right)** after 6 hours of ARS ($t_{12} = 2.312$, $p = 0.0394$, unpaired t-test, two-tailed; Ki16425 + NaCl: $t = 0.590$, $p = 0.57$, One sample t test and Ki16425 + TMZ: $t = 2.606$, $p = 0.0404$, one sample t test, $n = 7$ mice per group). **α.** Quantification of Ki-67⁺ cells in the DG ($t_{12} = 2,356$, $p = 0.0349$, unpaired t-test, two- tailed, $n = 7$ per group). **β.** Experimental design. **γ.** Histogram of the percentage of marble buried after 20minute-session of MBT ($F_{2,18} = 1.038$, $p = 0.89$, one-way ANOVA, $n = 7$ mice per group). **δ.** Histogram of the latency to the first bite after 6 minutes of NSFT ($F_{2,18} = 3.846$, $p = 0.0407$, One-way ANOVA; Vehicle+NaCl vs Ki16425+NaCl, $p = 0.033$, Ki16425+NaCl vs Ki16425+TMZ, $p = 0.025$, $n = 7$ mice per group). **ε.** Quantification of Ki-67⁺ cells in the DG ($F_{2,18} = 6,169$, $p = 0.0091$, One-way ANOVA; Vehicle+NaCl vs K16425+NaCl, $p = 0.06$, Ki16425+NaCl vs Ki16425+TMZ $p = 0.007$, $n = 7$ mice per group). **ζ.** Quantification of BrdU⁺/NeuN⁺ cells in the DG (DG, $F_{2,18} = 3,514$, $p = 0.05$, One-way ANOVA; Vehicle+NaCl vs Ki16425+NaCl, $p = 0.049$, Ki16425+NaCl vs Ki16425+TMZ, $p = 0.16$, $n = 7$ mice per group). Linear regression, r^2 and p values are indicated in the graphs when significant correlations were found. Histograms show average \pm SEM. * $p < 0.05$; ** $p < 0.01$; *** $p < 0.001$; ns: not significant. Comparison between the group mean and the hypothetical value of 0.5, to assess anxiety withing each group are shown within each histogram bar. One-sample t-test. #: $p < 0.05$; ##: $p < 0.01$. Source data are provided as a Source Data file.

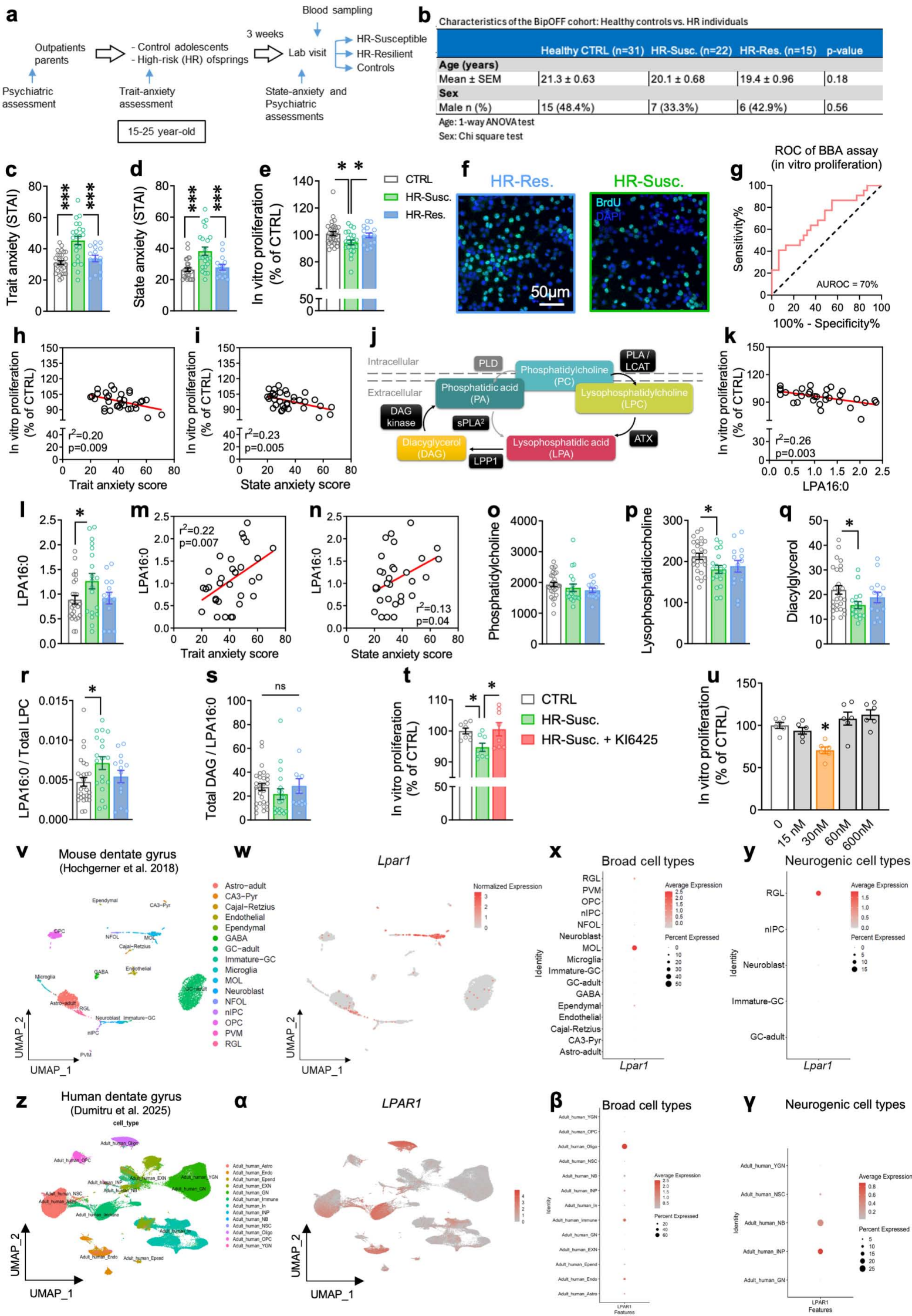
Fig. 4: Platelet depletion reduces circulating LPA16:0 and increases stress resilience and

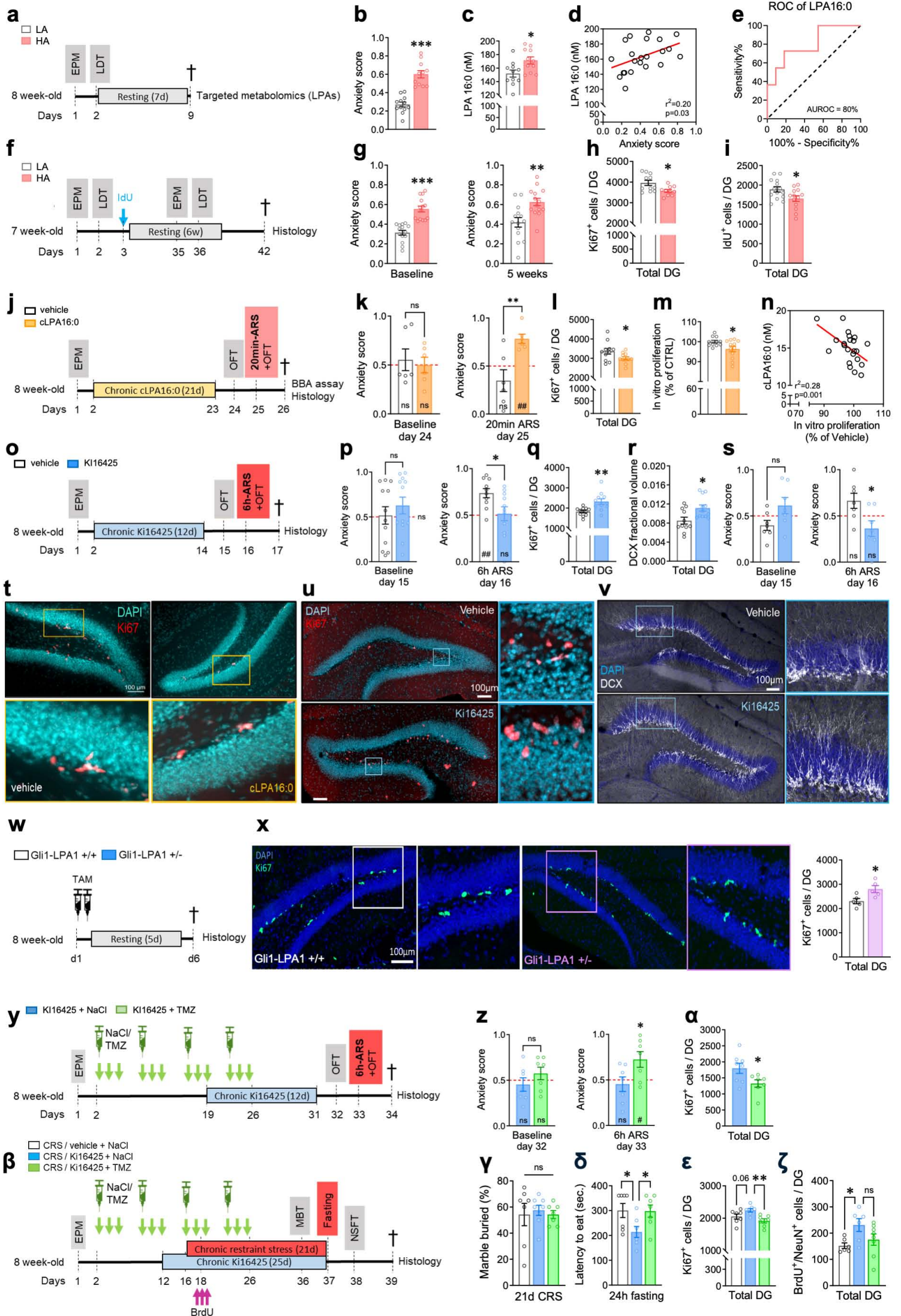
adult neurogenesis. a. Table showing platelets count and levels of LPAs in activated platelet-rich plasma from mice treated with an anti-platelet serum (n=4) or control serum (n=4) for 2 days. Data shows platelets counts for sampled pooled for all 4 mice per group. **b.** Experimental design. **c.** Histograms of the anxiety score of mice injected with control (white) or anti-platelet serum (purple) after 20 days of treatment under **(left)** baseline conditions (t14 = 2.922, p = 0.0011, unpaired t-test, two-sided; control: t = 1.651, p = 0.14, One sample t test and anti-platelet: t = 2.610, p = 0.035, One sample t test, n = 8 mice per group) and **(right)** after 6 hours of ARS (t14 = 5.005, p = 0.0002, unpaired t-test, two-tailed; control: t = 11.29, p = 2.9E-05, One sample t test and anti-platelet: t = 0.852, p = 0.42, One sample t test, n = 8 mice per group). **d.** Quantification of Ki- 67⁺ cells in the DG (t14 = 2,452, p = 0.0279, unpaired t-test, two-sided, n = 8 per group). Histograms show average \pm SEM. * p<0.05; ** p<0.01; *** p<0.001; ns: not significant. Comparison between the group mean and the hypothetical value of 0.5, to assess anxiety withing each group are shown within each histogram bar. One-sample t-test. #: p<0.05; ##: p<0.01. Source data are provided as a Source Data file.

Editorial summary: This study shows that in anxiety, circulating LPA16:0 produced by platelets inhibits adult hippocampal neurogenesis, resulting in increased susceptibility to stress and depression. These results support LPA16:0 as a potential therapeutic target for mood disorders.

Peer review information: *Nature Communications* thanks the anonymous reviewers for their contribution to the peer review of this work. A peer review file is available.





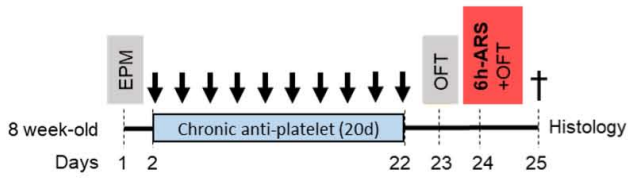
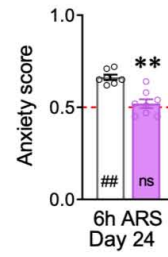
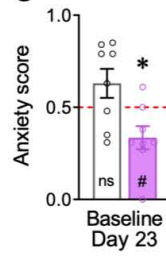


a

Effect of the anti-platelets on platelets count and LPAs levels

| | aPRP-Control serum | aPRP-Anti-platelet serum |
|---|--------------------|--------------------------|
| Platelets count ($\times 10^3 / \mu\text{L}$) | 756 | ND |
| LPA16:0 (μM) | 7,74 | ND |
| LPA16:0 Cyclic (μM) | 221,94 | 185,01 |
| LPA18:0 (μM) | 0,49 | 1,92 |
| LPA18:1 (μM) | 19,88 | 16,66 |
| LPA18:2 (μM) | 204,64 | 243,24 |
| LPA20:4 (μM) | 170,63 | 101,84 |

ND: Not Detected

b**c****d**